

Accepted Manuscript

# *Journal of the Geological Society*

## Constraining reducing conditions in the Prague Basin during the late Silurian Lau/Kozlowskii extinction event

Lindsay J. Allman, Chelsie N. Bowman, Jiří Frýda, Nevin P. Kozik, Jeremy D. Owens & Seth A. Young

DOI: <https://doi.org/10.1144/jgs2023-108>

To access the most recent version of this article, please click the DOI URL in the line above. When citing this article please include the above DOI.

This article is part of the Chemical Evolution of the Mid-Paleozoic Earth System and Biotic Response collection available at: <https://www.lyellcollection.org/topic/collections/chemical-evolution-of-the-mid-paleozoic-earth-system>

Received 30 June 2023

Revised 20 November 2023

Accepted 18 December 2023

© 2024 The Author(s). Published by The Geological Society of London. All rights reserved. For permissions: <http://www.geolsoc.org.uk/permissions>. Publishing disclaimer: [www.geolsoc.org.uk/pub\\_ethics](http://www.geolsoc.org.uk/pub_ethics)

Supplementary material at <https://doi.org/10.6084/m9.figshare.c.7008107>

### **Manuscript version: Accepted Manuscript**

This is a PDF of an unedited manuscript that has been accepted for publication. The manuscript will undergo copyediting, typesetting and correction before it is published in its final form. Please note that during the production process errors may be discovered which could affect the content, and all legal disclaimers that apply to the journal pertain.

Although reasonable efforts have been made to obtain all necessary permissions from third parties to include their copyrighted content within this article, their full citation and copyright line may not be present in this Accepted Manuscript version. Before using any content from this article, please refer to the Version of Record once published for full citation and copyright details, as permissions may be required.

# **Constraining reducing conditions in the Prague Basin during the late Silurian Lau/Kozlowskii extinction event**

**Lindsi J. Allman<sup>1\*</sup>, Chelsie N. Bowman<sup>1</sup>, Jiří Frýda<sup>2,3</sup>, Nevin P. Kozik<sup>1</sup>, Jeremy D. Owens<sup>1</sup>, and Seth A. Young<sup>1</sup>**

<sup>1</sup>Department of Earth, Ocean & Atmospheric Science | National High Magnetic Field Laboratory, Florida State University, Tallahassee, FL, USA.

<sup>2</sup>Faculty of Environmental Sciences, Czech University of Life Sciences Prague, Prague, Czech Republic.

<sup>3</sup>Czech Geological Survey, Klárov 3/131, 118 21 Prague 1, Czech Republic.

ORCID: LJA: 0000-0001-8577-6788; CNB: 0000-0001-9052-7014; JF: 0000-0003-2410-3293; NPK: 0000-0001-7759-7552; JDO: 0000-0002-0530-2177; SAY: 0000-0001-6885-4780

\*Corresponding author: Lindsi Allman ([lja15@fsu.edu](mailto:lja15@fsu.edu))

## Abstract

The Silurian was marked by repeated extinctions, carbon cycle volatility, and significant intervals of climatic change. The most notable of these events were the Ludfordian Lau/Kozlowskii extinction and associated Mid-Ludfordian Lau carbon isotope excursion, both of which have been linked to a period of global cooling and expanded reducing conditions in the global oceans. Here we present new data that characterize marine paleoredox conditions of the Prague Basin, a peri-Gondwanan terrane. This study utilizes iodine-to-calcium ratios to assess local redox conditions in a shallow water carbonate succession and iron speciation and redox-sensitive trace element concentrations to assess local redox conditions of a deeper water sequence. Consistently low values of I/Ca in the shallow water section suggest either persistent local low oxygen conditions or possibly diagenetic overprinting. Iron speciation data suggest that bottom water redox conditions in the deeper shelf setting were consistently anoxic with possible intermittent euxinia. Concentrations of redox-sensitive trace elements consistently higher than upper continental crust values also indicate persistent reducing conditions in the deeper part of the basin. These local redox proxy data from the Prague Basin, including trends in new pyrite sulfur isotope ( $\delta^{34}\text{S}_{\text{pyr}}$ ) data, are consistent with findings that expansion of anoxic and/or euxinic oceanic conditions occurred. These data, derived from a mid-paleolatitude marine setting, fill an important gap in our current global dataset from this interval of the late Silurian.

**Supplementary Material:** All geochemical data reported and discussed herein are available in supplemental data tables.

In the last three decades the Silurian has been recognized as an extremely dynamic period in Earth history. An oscillatory climatic transition from the icehouse of the Late Ordovician to the greenhouse conditions of the Devonian (e.g., Jeppsson, 1990; Bickert et al., 1997; Cramer and Saltzman, 2007) was accompanied by repeated marine extinctions and faunal reorganizations (e.g., Jeppsson, 1998; Crampton et al., 2016), extreme carbon cycle volatility (e.g., Kaljo et al., 1997; Saltzman, 2001, 2002; McAdams et al. 2019), and notable variations in marine redox conditions (Bowman et al., 2019, 2020, 2021; Rose et al., 2019; Young et al., 2019, 2020; del Rey et al., 2020, 2023; Frýda et al., 2021a, b; Zhang et al., 2022). Among

those recurring extinction events was the Ludfordian (Ludlow Epoch) Lau/Kozlowskii extinction (LKE), which was the most severe in the Silurian and at least the tenth most severe in Earth history with a loss of ~23% of marine genera (Sepkoski, 1996; Bond and Grasby, 2017). The Lau/Kozlowskii extinction is named after the ‘Lau bioevent’ in conodonts from carbonate platform successions (Jeppsson, 1990) and the ‘Kozlowskii bioevent’ in graptolites from deeper-water shales (Koren, 1993; Urbanek, 1993). The LKE is associated with the mid-Ludfordian Lau carbon isotope excursion (Lau CIE – also known as the MLCIE), one of the highest magnitude CIEs in the Phanerozoic, with peak excursion values typically between +5 to +9‰ (Munnecke et al., 2003; Calner, 2008; Saltzman and Thomas, 2012). The marine extinction slightly pre-dates the onset of the Lau CIE, but both are now hypothesized to be caused by an expansion of reducing conditions in the global oceans (Munnecke et al., 2003; Stricanne et al., 2006; Bowman et al., 2019; Frýda et al., 2021b). This is evidenced not only by geochemical proxy data such as sulfur isotopes (Bowman et al., 2019), uranium isotopes (del Rey et al., 2020, 2023), and barium isotopes (Zhang et al., 2022), but also by the curiously asynchronous nature of the LKE. Documented extinctions in benthic and nektonic taxa, such as brachiopods (Talent et al., 1993; Mergl et al., 2018), fish (Eriksson et al., 2009), polychaetes (Tonarová et al., 2012), cephalopods (Manda, 2008), trilobites (Manda and Frýda, 2014), and conodonts (e.g., Jeppsson and Aldridge, 2000), precede extinctions in planktic fauna, such as graptolites (Koren, 1993; Urbanek, 1993) and acritarchs (Stricanne et al., 2006), suggesting that reducing conditions expanded from deeper to shallower marine waters (Bowman et al., 2019; Frýda et al., 2021b).

Recent analysis of seawater surface temperature changes (Frýda et al., 2021b) using conodont apatite  $\delta^{18}\text{O}$  records from different regions located in temperate (Prague Basin and Carnic Alps) as well as tropical (Gotland) paleolatitudes points to significant global cooling during the Lau CIE. The marked decline of sea surface temperatures (inferred from the positive shift in  $\delta^{18}\text{O}_{\text{apatite}}$  of at least 3‰) recorded in temperate-water areas of the Prague Basin and Carnic Alps (peri-Gondwana) as well as in the tropical areas of Baltica (Laurussia) and Australia (Gondwana), coupled with a significant eustatic sea-level fall recorded by sequence stratigraphy on all corresponding paleocontinents point to glaciation (Mid-Ludfordian glaciation—see Frýda et al., 2021b) in polar and subpolar Gondwana.

To date, the majority of marine redox proxy data for the Lau/Kozlowskii extinction has come from tropical epicontinental basins of the paleocontinents Baltica and Laurentia (e.g., Bowman et al., 2019, 2020, 2021; del Rey et al., 2020). Recently studies published by Frýda

et al. (2021b) Zhang et al. (2022), and del Rey et al. (2023) have reported the first marine redox proxy dataset of redox-sensitive trace element concentrations and barium and uranium isotopes, respectively, from temperate paleolatitudes of peri-Gondwanan terrane, Perunica (Kosov Quarry in Czech Republic; Fig. 1B). Here we present additional shale-based proxy records from the Kosov Quarry to assess local to regional deep shelf redox conditions in more detail, including pyrite sulfur isotope ( $\delta^{34}\text{S}_{\text{pyr}}$ ), iron speciation, and redox-sensitive trace element concentration data. Also presented herein are iodine-to-calcium ratios and pyrite sulfur isotope ( $\delta^{34}\text{S}_{\text{pyr}}$ ) redox proxy data from the shallow shelf carbonate succession of the Mušlovka Quarry Section in the Prague Basin. Key information and references for local redox proxy dynamics are summarized in Fig. 2. Using these paleoredox proxy datasets, we reconstruct how regional redox conditions of the Prague Basin changed throughout the Ludfordian Stage with respect to both the LKE and Lau CIE. The data and environmental reconstructions discussed here are of particular interest because they offer a detailed perspective on the local expression of these global environmental changes from the mid-paleolatitude Gondwanan margin.

## Geologic Setting and Biostratigraphy

The Mušlovka Quarry and Kosov Quarry (no. JF195) sections are both near modern-day Prague in the Czech Republic and were deposited in the Prague Basin of the Barrandian Terrane located between 25 – 30°S of the equator during the Ludfordian (Fig. 1A; Lehnert et al., 2007; Frýda and Manda, 2013; Tasáryová et al., 2014a). This basin formed on submerged continental crust inundated by shallow seas and bounded by deeper marine settings. The Barrandian crustal block is debated to have been either an accretion of peri-Gondwanan terranes or the small microcontinent often called Perunica (Havlíček et al., 1994; Cocks and Torsvik, 2002; Stampfli et al., 2002). The Central Bohemian region of the modern Czech Republic provides a variety of outcrops with a diversity of marine lithofacies deposited during the late Silurian, ranging from shallow shelf coarse-grained carbonate facies to deep shelf graptolite shale/mudstone successions. The Ludfordian strata of the Prague Basin make up the upper Kopanina Formation, which at the Mušlovka Quarry is composed of shallow shelf carbonate facies (Figs. 3A–E, 4) and at the Kosov Quarry is composed of deeper water interbedded carbonates/marls and shales (Figs. 3F–G, 5, 6).

There was active faulting and volcanism in the Prague Basin during the late Silurian that led to the development of rapid facies changes over short distances due to variable subsidence

and uplift rates (Havlíček and Štorch 1990; Kříž, 1991, 1992; Manda and Kříž, 2006; Lehnert et al., 2007; Frýda and Manda, 2013; Tasáryová et al., 2018). This early to middle Paleozoic tectonic activity is thought to be associated with continental rifting in the Barrandian Terrane that never reached an oceanic stage with the production of mid-ocean ridge basalts (e.g., Štorch, 1998; Tasáryová et al., 2018). In particular, the Kosov Quarry section (Fig. 1B) was located near the Silurian Kosov Volcanic Center deposited in the latest Wenlock interval. Volcanic activity occurred in this area from the Homeric through Gorstian stages of the middle-late Silurian (Tasáryová et al., 2014). The volcanic rocks are overlain by Ludfordian marine sedimentary strata. This includes the interbedded shales/mudstones and carbonates of Kosov Quarry that are the remnants of an offshore deep shelf setting (Lehnert et al., 2007). This was followed by the Variscan Orogeny that formed during the closure of the Rheic Ocean from the Devonian to the Pennsylvanian as part of the assembly of Pangaea (Röhlich, 2007; Tasáryová et al., 2018). The strata of the Prague Basin (Ordovician to Middle Devonian) are thought to have been buried between 1 to 4 km during the Variscan Orogeny (Vacek and Žák, 2019). By the Cretaceous, this region was dominated by variable extensional and compressional tectonics related to the motion between European and African plates that continued into the Neogene (Hrubcová et al., 2010). The collision of these two plates led to the formation of the Alpine/Carpathian Orogeny and the uplift and exposure of the Paleozoic strata of the Barrandian Terrane (Hrubcová et al., 2010).

The outcrops in this region serve as a reference for peri-Gondwanan biostratigraphy in the middle Paleozoic, with detailed work done on Silurian through early Devonian successions, in particular (Havlíček and Štorch 1990; Kříž, 1991, 1992). Given the presence of both peri-Gondwanan and Baltic-Avalonian-Laurentian fauna, the Prague Basin was well connected to the Rheic Ocean (Kříž, 1999, 2008; Manda, 2008). The age of deposition for the Mušlovka Quarry section has been well-constrained by conodonts (Kříž and Schönlaub, 1980; Slavík et al., 2014) and by graptolites and conodonts for the Kosov Quarry (Štorch, 1995; Frýda et al., 2021b).

The sampled interval of the Kopanina Formation at Mušlovka Quarry encompasses the *Neocucullograptus inexpectatus* graptolite zone in the lowest part of the section, the *Neocucullograptus kozlowskii* zone—the last appearance datum of which defines the Kozlowskii graptolite extinction, and the *Monograptus latilobus* and *Monograptus fragmentalis* graptolite zones in the upper part of the section (Fig. 4; Urbanek, 1993; Štorch, 1995; Manda et al., 2012; Manda and Frýda, 2014). Also present within the lower part of the

section is the *Polygnathoides siluricus* conodont zone, the practical last appearance datum of which defines the Lau conodont extinction, and the *P. latialata* – *O. snajdri* interval zone in the upper part of the section (Fig. 4; Kříž and Schönlaub, 1980; Jeppsson, 2005). The Mušlovka Quarry section is ~17 m of exposed shallow-water carbonates of the Kopanina Formation located outside of Prague, Czech Republic (Lehnert et al., 2003, 2007; Fig. 2A–E, 4). The lowest ~4 m of the sampled interval is a wackestone to packstone with cephalopods, echinoderm fragments, brachiopods, sponges, ostracodes, and graptolites. The upper 13 m of the section is mudstone to wackestone with fewer and less diverse macrofossils such as echinoderm fragments, brachiopods, cephalopods, and sponges. There are three intervals of flat-pebble conglomerate facies in the upper part of the section (e.g., 4.5 – 5.0 m, 6.0 – 6.5 m, and 8.0 – 13.0 m levels) made up of ~10 cm long, 2–3 cm thick clasts (Fig. 2B–D). The clasts in the upper two flat-pebble conglomerate intervals are often coated grains with sub-concentric laminations (Fig. 2B, C). A heavily dolomitized interval is present in the middle of the measured section from 3.0 to 13.0 meters (Fig. 2D, E). The likely once micritic matrix of the flat-pebble conglomerate intervals are completely altered with the growth of subhedral to euhedral dolomite and the wackestone to grainstone flat-pebble conglomerate clasts are partially dolomitized. The uppermost 1.5 m of the section are notably laminated and interbedded lime mudstones and black shale. Finely disseminated pyrite is also found throughout the section (e.g., Fig. 2E) with some intervals having secondary pyrite present within common secondary calcite veins and infilling bioclastic intraparticle pore spaces.

In the Kosov Quarry, the base of the section begins in the *N. inexpectatus* graptolite zone above which is the *N. kozlowskii* graptolite zone (Figs. 5, 6). Following this is the *Pristiograptus dubius postfrequens* partial-range interval graptolite zone. In the upper part of the section is the combined *M. latilobus* – *Slovenograptus balticus* zone and lastly the *M. fragmentalis* zone. The *P. siluricus* conodont zone is also at the base of the section followed by *P. latialata* – *O. snajdri* interval zone, and *O. crista* zone (Figs. 5, 6; Lehnert et al., 2007; Frýda et al., 2021b). Based on vitrinite reflectance of Silurian graptolites in the Prague Basin of 0.78 to 1.53%, which correspond to conodont color alteration index values of 2.5 to 3.5, burial temperatures likely ranged from 100° to 160°C (Epstein et al., 1977; Suchý et al., 2002; Hackley and Cardott, 2016). Several geochemical aspects of the Lau CIE have been analyzed from this section including continental weathering, paleoclimate, and marine paleoredox proxies such as  $\delta^7\text{Li}$ ,  $\delta^{13}\text{C}_{\text{carb}}$ ,  $\delta^{13}\text{C}_{\text{org}}$ ,  $\delta^{18}\text{O}_{\text{carb}}$ ,  $\delta^{34}\text{S}_{\text{pyr}}$ ,  $\delta^{34}\text{S}_{\text{CAS}}$ ,  $^{44/40}\text{Ca}$ ,  $^{87}\text{Sr}/^{86}\text{Sr}$ ,

$\delta^{138}\text{Ba}$ ,  $^{187/188}\text{Os}$ ,  $\delta^{238}\text{U}$ , and some trace elements (Lehnert et al., 2007; del Rey et al., 2023; Frýda and Manda, 2012; Farkaš et al., 2016; Frýda et al. 2021a, b; Sproson et al., 2022; Zhang et al., 2022). The Kosov Quarry section begins with a series of dark brown and grey, finely laminated shales which quickly become interbedded with marly limestone deposits. Within the section, there is an unconformity representative of a stratigraphic gap associated with a flat-pebble conglomerate bed. As the section continues, the shale lithology becomes lighter in color and more calcareous, limestone interbeds also become more numerous. This increase in carbonate content here at Kosov Quarry is due to an overall shallowing trend in eustatic sea level during the glaciation (Lehnert et al., 2007; Gocke et al., 2013; Frýda et al., 2021b). The top of the section contains a cephalopod limestone bed, likely deposited in a sea level lowstand (Ferretti and Kříž, 1995) and tuffites are dispersed within the section. The complicated stratigraphy in Kosov Quarry is due to repetitive local sea-level changes combined with increasing accommodation space due to subsidence and carbonate platform destruction during sea-level lowstand (Lehnert et al., 2007; Manda et al., 2012; Gocke et al., 2013; Frýda and Manda, 2013; Frýda et al., 2021a, b).

## Materials and Methods

### Sample Preparation

Samples were collected and described in approximately 0.5-meter increments through the Kopanina Formation of the Mušlovka Quarry and Kosov Quarry sections in the Prague Basin, Czech Republic (Lehnert et al., 2007). Where possible, intervals that were notably weathered or had obvious diagenetic influences (e.g., secondary calcite veins, notable recrystallization, iron-oxide staining, pyrite nodules) were avoided during sampling. For the Mušlovka Quarry carbonate samples, weathered edges and large, secondary calcite veins were removed using a water-based diamond blade saw. Representative samples from each section were slabbed for thin section analysis. From each carbonate sample approximately 1 g of powder was preferentially micro-drilled from micritic matrix (except in the case of grainstones) for  $\delta^{13}\text{C}_{\text{carb}}$  and I/Ca analyses. For all other geochemical analyses, 200 – 300 g of sample was crushed and powdered using an alumina ceramic disc mill with a SPEX8510 ShatterBox. The shale samples collected at the Kosov Quarry section were first cleaned via the removal of weathered surfaces using an ultrasonic bath in deionized water. The samples were then

crushed using an agate mortar and pestle to produce 7 to 10 grams of powdered rock. Splits of these powders were used for various geochemical analyses described below.

### **Carbon Isotopes**

For carbonate carbon isotope analyses, between 0.2 – 1 mg of powder was weighed out from each sample. The powders were acidified with 100%  $\text{H}_3\text{PO}_4$  at 25 °C for 24 h. Stable carbon and oxygen isotopes of the evolved  $\text{CO}_2$  gas were then analyzed using a ThermoFinnigan Gas Bench II Autocarbonate device coupled to a ThermoFinnigan Delta Plus XP isotope-ratio mass spectrometer (IRMS) at the National High Magnetic Field Laboratory (NHMFL) at Florida State University. Analytical precision of  $\delta^{13}\text{C}_{\text{carb}}$  is  $\pm 0.05\text{‰}$  ( $1\sigma$ ) and  $\delta^{18}\text{O}_{\text{carb}}$  is  $\pm 0.1\text{‰}$  ( $1\sigma$ ) based on long-term, replicate analysis of NBS-19 and other laboratory standards.

Organic carbon isotope analyses were done on a subset of samples from the Mušlovka Quarry and all shale interbeds from the Kosov Quarry. Between 2 – 4 g of carbonate or shale powder was accurately weighed and then acidified at least three times with 6 M HCl to remove carbonate minerals. The insoluble residues were then rinsed in ultrapure (deionized, 18.2 M $\Omega$ ) water until a neutral pH was reached, then dried overnight in an oven at 70 °C. The residues from each sample were homogenized in agate mortars and weighed into tin cups for analysis. The organic carbon isotope values were measured using a Costech Elemental Analyzer coupled to a ThermoFinnigan Delta Plus XP IRMS via an open-split Conflo III at the NHMFL. The weight percent of total organic carbon (TOC) was calculated based on the comparison of voltages for the ion beam intensity of mass 44 and the area all integration for masses 44, 45, 46 for  $\text{CO}_2^+$  between the unknown samples and the known weight percent of the gravimetric standard acetanilide. Analytical precisions of  $\pm 0.2\text{‰}$  ( $1\sigma$ ) for  $\delta^{13}\text{C}_{\text{org}}$  and  $\pm 0.7\%$  ( $1\sigma$ ) for % C are based on long-term, replicate analysis of laboratory standards calibrated to IAEA standards. All carbon isotope data is reported in standard delta notation ( $\delta$ ) with units of per mil (‰) relative to the Vienna Pee Dee Belemnite (V-PDB) standard.

### **Sulfur Isotopes**

Carbonate-associated sulfate (CAS) extractions for sulfur isotope analysis were performed with minor modifications from procedures outlined by Wotte et al. (2012) on the carbonate samples from Mušlovka Quarry. For each sample, between 80 to 250 g of powdered carbonate was rinsed three times in a 10% NaCl solution and three times in ultrapure (deionized, 18.2 M $\Omega$ ) water for ~12 h per rinse to remove soluble, secondary sulfate minerals

(Edwards et al., 2019). Samples were then acidified through titration of 6 M HCl for no more than 2 h per sample in an attempt to avoid pyrite oxidation. The insoluble residues were then separated from the acidified solutions via centrifugation. The acidified solutions were brought up to a pH of 10 with NaOH; the precipitates from this reaction were then removed through vacuum filtration. Post-filtration, remaining solutions were re-acidified to a pH of 4 using a few drops of 12 M HNO<sub>3</sub>. Excess BaCl<sub>2</sub> was added to each sample solution and dissolved sulfate was allowed to precipitate as barite (BaSO<sub>4</sub>) over 72 h. The barite was then rinsed in ultrapure water and dried.

Chromium reducible sulfides (CRS) were extracted from the insoluble residues remaining from the CAS extraction of the Mušlovka Quarry samples and from the powdered Kosov Quarry samples based on modified protocols from Canfield et al. (1986) and Brüchert and Pratt (1996). Residues were reacted with a 70:30 mixture of 12 M HCl and 1 M CrCl<sub>3</sub> in an N<sub>2</sub> purged flask. Evolved H<sub>2</sub>S gas was then bubbled into AgNO<sub>3</sub> to precipitate Ag<sub>2</sub>S. The total amount of precipitant was gravimetrically determined to calculate the concentration of pyrite in each sample, assuming quantitative stoichiometry. Approximately 350 µg of barite (CAS) or silver sulfide (CRS) was weighed into tin cups with excess V<sub>2</sub>O<sub>5</sub> for sulfur isotope analysis using a Thermo Isolink Elemental Analyzer coupled via open-split Conflo IV to a Thermo Delta V Plus IRMS at the NHMFL. All sulfur isotope results are reported in standard delta notation (δ) with units of per mil (‰) relative to the Vienna Cañon Diablo Troilite (V-CDT) standard. Analytical precision is ± 0.2‰ (1σ) based on long-term, replicate analysis of IAEA-S-3 and calibrated internal lab standards.

### **Iodine-to-Calcium Ratios**

I/(Ca+Mg) ratios, hereafter referred to as I/Ca, were measured for the Mušlovka Quarry samples at the NHMFL using an Agilent 7500cs quadrupole inductively coupled plasma mass spectrometer (ICP-MS) according to standard methods (e.g., Lu et al., 2010, 2017; Hardisty et al., 2014, 2017). Approximately 2 – 5 mg of micro-drilled carbonate powder was acidified with 3% HNO<sub>3</sub> to dissolve all carbonate material. Samples were vortexed and centrifuged to ensure complete dissolution of carbonate and separation from insoluble residue. The supernatant was then diluted to a ~50 ppm Ca + Mg solution in a matrix of 2% HNO<sub>3</sub>. Samples were rerun until a consistent matrix of 50 ppm ±5 ppm Ca + Mg was achieved. Calibration standards were made each day by serial dilution of a 10 ppm iodine ICPMS standard from High Purity Standards with a similar matrix of ~50 ppm Ca + Mg. Analyses

were performed on the ICP-MS at the NHMFL within 2 h of acidification (due to the volatility of iodine). The precision of  $^{127}\text{I}$  is typically better than 2% and is not reported separately for individual samples. Standard deviation in counts per second (cps) for three blanks in a row is typically below 300 cps, and the sensitivity for a 1 part per billion standard is typically 60,000–120,000 cps depending on the instrument set-up each day (that is, sensitivity varies day to day, but the geostandards document consistent ratios). The long-term accuracy of this procedure was based on replicate analysis of internal FSU-NHMFL laboratory reference materials KL 1-2 ( $\pm 0.50 \mu\text{mol/mol}$ ) and KL 1-4 ( $\pm 0.46 \mu\text{mol/mol}$ ) based upon Hardisty et al. (2014) and previous work from the Geochemistry Group at the National High Magnetic Field Laboratory (Lowrey et al., 2018; Bowman et al., 2020; Kozik et al., 2022; Lindskog et al., 2023). I/Ca ratios, and the notation used throughout, are commonly reported as I/(Ca+Mg) to account for variable carbonate mineralogy and particularly dolomitization in ancient carbonates (e.g., Hardisty et al., 2014, 2017; Lu et al., 2017, 2018).

### **Iron geochemistry**

Based on the methods outlined in Poulton and Canfield (2005), approximately 100 mg of powdered rock from each of the Kosov Quarry shale samples, interbedded carbonates were not analyzed, were weighed into 15 mL centrifuge tubes. A solution of 1M sodium acetate was buffered to a pH of 4.5 to extract Fe associated with carbonate phases ( $\text{Fe}_{\text{carb}}$ ): 10 mL of sodium acetate was then added to each sample, which were placed on a shaker table for 24 hours. The next extraction process removed iron associated with crystalline oxides ( $\text{Fe}_{\text{ox}}$ ) by adding 0.29 M sodium dithionite buffered with 0.35M acetic acid and 0.2 M sodium citrate to each sample, which were then agitated for 2 hours. Lastly, Fe in magnetite ( $\text{Fe}_{\text{mag}}$ ) was selectively extracted using 0.2M ammonium oxalate and 0.17M oxalic acid buffered to a 3.2 pH added to each sample and shaken for 6 hours. An aliquot of the supernatant was saved from each extraction step, diluted with 2%  $\text{HNO}_3$ , and analyzed on the Agilent 7500cs quadrupole ICPMS at the NHMFL. Highly reactive iron ( $\text{Fe}_{\text{HR}}$ ) is calculated by summing  $\text{Fe}_{\text{carb}} + \text{Fe}_{\text{ox}} + \text{Fe}_{\text{mag}} + \text{Fe}_{\text{pyr}}$ . The sequential Fe method has a reproducibility of  $\sim \pm 7\%$ .  $\text{Fe}_{\text{pyr}}$  was determined by weighing the  $\text{Ag}_2\text{S}$  precipitate from chromium reducible sulfide extraction (CRS, mentioned above) and then quantitative stoichiometry was used to calculate  $\text{Fe}_{\text{pyr}}$ .

### **Major and Trace Element Geochemistry**

A multistep acid digestion procedure was used to dissolve each of the powdered shales from the Kosov Quarry, importantly, interbedded carbonates were not analyzed. Powdered samples were weighed into Teflon beakers and then digested in various combinations of trace metal clean concentrated HNO<sub>3</sub>, HCl, and HF. The samples were kept on hot plates at ~120 – 160°C, typically overnight, then dried down each time before a new acid solution was added. Trace metal clean H<sub>2</sub>O<sub>2</sub> was used to oxidize organic matter when necessary. After complete dissolution, the samples were dried down and re-dissolved in 2% HNO<sub>3</sub> before being diluted and run on an Agilent 7500cs quadrupole ICPMS for major and trace element concentrations at the NHMFL. USGS standards SDO-1, SCO-1, and SGR-1 were dissolved along with the samples and were within analytical ranges for reported elements. Results are reported in ppm with analytical precision of ± 5% or better for iron, aluminum, manganese, vanadium, uranium, and molybdenum. Blanks were below detection limit. Trace element results are plotted as absolute concentrations, carbonate-corrected concentrations, and TOC-normalized concentrations (Fig. 6). Manganese concentrations are reported and discussed in the text as carbonate-corrected values; V, U, & Mo are reported and discussed as carbonate-corrected values normalized to each sample's total organic carbon content. We also present enrichment factor data for U & Mo (Fig. 8). Trace metal enrichment factors are calculated as  $X_{EF} = [(X/Al)_{\text{sample}}/(X/Al)_{\text{PAAS}}]$ , where X is the concentration in each sample of the element in question (here either U or Mo), Al is the concentration of aluminum in the sample. The quotient of  $X/Al_{\text{sample}}$  is then normalized to the ratio of X/Al in post-Archean average shale (PAAS; Taylor and McLennan, 1995). Samples with values above 3 are considered to have detectable authigenic enrichment and values above 10 have substantial enrichment (Algeo and Tribovillard, 2009).

## Results

### Mušlovka Quarry Sedimentological and Geochemical Results

The Lau CIE has been previously documented in the Mušlovka Quarry section by Lehnert et al. (2003, 2007) as a ~ +5‰ magnitude excursion in  $\delta^{13}\text{C}_{\text{carb}}$  just above the *N. kozłowskii* zone. Here, we document an approximately parallel excursion in  $\delta^{13}\text{C}_{\text{org}}$  of ~ +4.2‰ in magnitude (Fig. 4A, black symbols). Pre-excursion baseline values of ~ -28.5‰ in  $\delta^{13}\text{C}_{\text{org}}$  quickly rose to a peak of -24.3‰ just above LAD of *P. siluricus* and before the peak in  $\delta^{13}\text{C}_{\text{carb}}$  values. Subsequently, the  $\delta^{13}\text{C}_{\text{org}}$  values steadily declined to a post-excursion baseline of ~ -29‰. I/Ca ratios were low throughout the section, consistently between 0 – 0.4

$\mu\text{mol/mol}$  in both carbonate mud matrix and in flat-pebble conglomerate clasts (Fig. 4D). There was one higher value of  $2.7 \mu\text{mol/mol}$  recorded from the upper part of the section, within the *M. fragmentalis* graptolite zone. The  $\delta^{34}\text{S}_{\text{CAS}}$  data was sparse, due to overall high concentrations of pyrite within this succession, with values only from the *N. inexpectatus* and *M. fragmentalis* graptolite zones, which ranged from  $+21.5$  to  $+24.8\text{‰}$  (Fig. 4B, red symbols). The  $\delta^{34}\text{S}_{\text{pyr}}$  values were relatively constant through the Mušlovka Quarry section, ranging from  $-30.6$  to  $-20.3\text{‰}$  with a slight negative trend moving upward through the section (Fig. 4B, black symbols).

### Kosov Quarry Sedimentological and Geochemical Results

The Lau CIE has been previously documented in the Kosov Quarry section by Lehnert et al. (2007), Frýda and Manda (2013), and Frýda et al. (2021a) as an  $\sim +8\text{‰}$  magnitude excursion in  $\delta^{13}\text{C}_{\text{carb}}$  in the *P. dubius postfrequens* partial-range interval and the combined *M. latilobus* – *S. balticus* graptolite zones just above the *N. kozlowskii* zone (Fig. 5A). Frýda et al. (2021a) also report a  $\sim +7\text{‰}$  magnitude excursion in  $\delta^{13}\text{C}_{\text{org}}$  through the same stratigraphic interval. The  $\delta^{13}\text{C}_{\text{org}}$  data collected for the present study from the Kosov Quarry shale interbed samples begin at pre-excursion baseline values  $\sim -30\text{‰}$  during the *M. inexpectatus* and *N. kozlowskii* graptolite biozones (Fig. 5A). Much of the rising limb of the excursion is missing/condensed due to an absence of shale in a short interval from about 50cm to 80cm above top of *N. kozlowskii* biozone. Subsequently, higher in the section shale interbeds are once more present in the *P. dubius postfrequens* graptolite zone; their corresponding  $\delta^{13}\text{C}_{\text{org}}$  values range from  $-24\text{‰}$  to  $-22\text{‰}$  in the peak interval of the Lau CIE. Around 20-meters above the base of the section  $\delta^{13}\text{C}_{\text{org}}$  values gradually begin to fall back to a post-excursion baseline of  $-30\text{‰}$  during the combined *M. latilobus* – *S. balticus* then *M. fragmentalis* graptolite zones. Newly gathered  $\delta^{13}\text{C}_{\text{org}}$  data fit well with stratigraphically high-resolution  $\delta^{13}\text{C}_{\text{org}}$  record by (Frýda et al., 2021a).

The  $\delta^{34}\text{S}_{\text{pyr}}$  data from the shale interbeds generally co-varies with the carbon isotope datasets generated from the Kosov Quarry. As with carbon isotope data,  $\delta^{34}\text{S}_{\text{pyr}}$  values from our Kosov Quarry shale samples are plotted along with  $\delta^{34}\text{S}_{\text{pyr}}$  values generated from the limestone interbeds of this section from Frýda et al. (2021a). The shale  $\delta^{34}\text{S}_{\text{pyr}}$  data from the base of the measured section show a wide range of values from  $-20\text{‰}$  to  $+15\text{‰}$  (Fig. 5B, red symbols). In general, the data from the shale interbeds is comparable to that of the limestone interbeds, despite the slightly wider range in isotope values. Within the upper *N. kozlowskii* graptolite

zone,  $\delta^{34}\text{S}_{\text{pyr}}$  values fall to  $\sim -15\%$ . Near the end of the LKE interval, in the lower *P. dubius postfrequens* graptolite zone,  $\delta^{34}\text{S}_{\text{pyr}}$  values increase to as much as  $+15\%$  (as compared to  $+7 - 8\%$  in limestone interbeds; Frýda et al., 2021a), and stay near this value throughout the interval of peak values of the Lau CIE. After this peak in  $\delta^{34}\text{S}_{\text{pyr}}$ , in the *M. latilobus* – *S. balticus* then *M. fragmentalis* graptolite zones, values sharply drop back to the  $-15\%$  pre-excursion value. The  $\delta^{34}\text{S}_{\text{pyr}}$  data from the limestone interbeds (Frýda et al., 2021a) document an additional excursion of  $\sim +30\%$  across the *M. latilobus* – *S. balticus* and *M. fragmentalis* graptolite zones that was not captured in our shale interbed dataset (Fig. 5B, red symbols).

The  $\text{Fe}_{\text{HR}}/\text{Fe}_{\text{T}}$  values ranged from 0.15 to 0.94 throughout the Kosov Quarry section, with most values above 0.38 (Fig. 6A).  $\text{Fe}_{\text{pyr}}/\text{Fe}_{\text{HR}}$  values were generally low throughout the section ranging from 0 – 0.3. Just before and during the LKE extinction, from the upper *M. inexpectatus* zone to the lower *P. dubius postfrequens* zone,  $\text{Fe}_{\text{pyr}}/\text{Fe}_{\text{HR}}$  values were notably higher between 0.61 – 0.93 (Fig. 6B).  $\text{Fe}_{\text{T}}/\text{Al}$  ratios ranged from 0.47 – 0.87 throughout the Kosov Quarry section (Fig. 6C). Values ranged between 0.5 to 0.7 during the *M. inexpectatus* and *N. kozlowskii* zones then increased to 0.8 during the lower *P. dubius postfrequens* graptolite zone. Values decreased to 0.5 – 0.7 throughout the middle and upper *P. dubius postfrequens*, before increasing to 0.9 in the *M. latilobus* – *S. balticus* zone.

Manganese concentrations are relatively low and consistent, most values are less than 400 ppm with a few data points near 750 ppm (Fig. 6D). Total organic carbon normalized vanadium concentrations are somewhat scattered, particularly in the lowest 10 m of the section in the *M. inexpectatus* and *N. kozlowskii* zones (Fig. 6E). At approximately 10 m, just above the upper boundary of the *N. kozlowskii* zone, there is a drop in average V/TOC from  $\sim 340$  to  $\sim 160$  ppm/wt%. U/TOC through the Kosov Quarry shows less scatter than that of V/TOC and there is a slight decrease in average values just above the upper boundary of the *N. kozlowskii* zone from 73 to 66 ppm/wt% (Fig. 6F).  $\text{U}_{\text{EF}}$  values range from 13 to 92 with an average value of 22 (Fig. 8). Mo/TOC ranged between 10 – 45 ppm/wt% (Fig. 6G). The average Mo/TOC values decrease mid-LKE, in the same interval as V & U, from 27 to 20 ppm/wt% (Fig. 6G).  $\text{MO}_{\text{EF}}$  values range from 8 to 68 with an average value of 16 (Fig. 8; see also: Supplemental Data Tables).

## Discussion

### Effects of Diagenesis on Primary Carbonate Geochemical Signatures at Mušlovka Quarry

All sedimentary strata experience some variety of post-depositional processes that have the potential to alter primary sedimentary textures and geochemical signatures, complicating the interpretation of proxy data. Due to processes such as recrystallization, carbonate rocks are particularly susceptible to potential diagenetic alteration. In the Mušlovka Quarry section, many of the samples show signs of obvious late diagenetic influence in thin section. From 3.0 to 13.0 meters in the sampled interval, almost all of the (presumably) once micritic matrix has been dolomitized (Fig. 3D, E). To a lesser extent coarser-grained components, such as the grainstone to wackestone flat-pebble conglomerate clasts, have also been partially dolomitized (Fig. 3D). The common occurrence of secondary calcite veins, steinkerns and partially recrystallized fossil allochems, and pressure dissolution features such as stylolites, throughout the Mušlovka Quarry section are reflective of this section's complicated tectonic and burial history (see Geologic Setting above).

General carbonate microfacies analysis of the Mušlovka Quarry section show that diagenetic processes notably affected primary carbonate textures. Conodont color alteration indices of 2.5 to 3.5 in the Mušlovka Quarry section indicate significant thermal influence on the studied strata (Epstein et al., 1977). Regardless, as with any carbonates, it is still important to assess if the geochemical trends in this study are possibly reflective of primary seawater conditions or are the result of post-burial processes, diagenetic or otherwise (e.g., Banner and Hanson, 1990; Railsback et al., 2003; Gill et al., 2008).

Here we use the geochemical data to assess carbonate diagenetic alteration. First, we use linear relationships observed in cross plots of geochemical proxy data, which have been extensively used to assess the degree of diagenetic alteration that sediments or rocks have experienced since deposition (Fig. 7, orange symbols; e.g., Lohmann, 1988; Hurtgen et al., 2002; Cramer and Saltzman, 2005; Swart and Eberli, 2005; Gill et al., 2008; Jones and Fike, 2013). Then we compare our data to modeled diagenetic changes in carbonate proxies based on recent work by Lau and Hardisty (2022). This includes modeled diagenetic changes under sediment- and fluid-buffered for meteoric water, oxidizing seawater, and reducing seawater (Fig. 7 A–C, E, F).

A notable correlation between  $\delta^{13}\text{C}_{\text{carb}}$  and  $\delta^{18}\text{O}_{\text{carb}}$  commonly indicates the partial resetting of carbon and oxygen isotope values from meteoric fluid flow. A cross plot of our  $\delta^{13}\text{C}_{\text{carb}}$  and  $\delta^{18}\text{O}_{\text{carb}}$  data (Fig. 7A) shows moderate correlation at Mušlovka Quarry, with an  $R^2$  value of 0.51. This is further supported by comparing the data from the Mušlovka Quarry to the modeled results of meteoric diagenesis in  $\delta^{13}\text{C}_{\text{carb}}-\delta^{18}\text{O}_{\text{carb}}$  space from Lau and Hardisty (2022). Meteoric diagenesis tends to drive both  $\delta^{13}\text{C}_{\text{carb}}$  and  $\delta^{18}\text{O}_{\text{carb}}$  more isotopically negative compared to their starting compositions. This can be clearly seen in the Mušlovka Quarry data which overlaps with the modeled isotopic changes from meteoric diagenesis (Fig. 7A).

Most of the I/Ca values from the Mušlovka Quarry section are at or near zero (i.e., below detection limit), as a result, the linear correlations are not particularly useful for assessing the effects of diagenesis on this proxy (Fig. 7B, C). The low I/Ca values could be indicative of diagenetic resetting due to the recrystallization of the original materials under the flow of reducing pore fluids. The I/Ca proxy has been previously shown to be very sensitive to diagenetic overprinting, which always shifts I/Ca ratios to lower values (e.g., Hardisty et al., 2017). Given the clear signal of meteoric diagenesis from  $\delta^{13}\text{C}_{\text{carb}}$  and  $\delta^{18}\text{O}_{\text{carb}}$  and the locally reducing conditions along the paleo-margin (see Local Redox discussion below), it is difficult to assess if the low I/Ca values are strictly due to diagenetic overprinting, a primary seawater signal of low oxygen content in the late Silurian water column, or some combination of both factors (Hardisty et al., 2017). Thus, our data is compared to modeled diagenetic changes in I/Ca compared to both  $\delta^{13}\text{C}_{\text{carb}}$  and  $\delta^{18}\text{O}_{\text{carb}}$  (Fig. 7B, C; Lau and Hardisty, 2022). As a result of the overlap in signals produced from modeling meteoric and reducing seawater fluid-buffered diagenetic changes in I/Ca- $\delta^{13}\text{C}_{\text{carb}}$  space, the cause of the low I/Ca values in the Mušlovka Quarry data remains somewhat unclear. When compared to the Lau and Hardisty (2022) modeling results in I/Ca- $\delta^{18}\text{O}_{\text{carb}}$  space though, the more negative  $\delta^{18}\text{O}_{\text{carb}}$  data from Mušlovka Quarry again suggest that meteoric diagenesis played a role in the extremely low I/Ca values (Fig. 7C). Beyond the comparison of our data to the modeled diagenetic effects on carbonate processes, the one data point at Mušlovka Quarry that was significantly above the detection limit ( $2.7 \mu\text{mol/mol}$ ) is located stratigraphically above the heavily dolomitized interval within this succession mentioned above, further supporting the hypothesis that diagenetic influence played a role in near zero the I/Ca values throughout most of the section.

The concentration of sulfate in the carbonate crystal lattice has also been shown to decrease during alteration as meteoric fluids have lower concentrations of both sulfate and iodate

compared to the original calcite (Gill et al., 2008; Sim et al., 2015; Hardisty et al., 2017). The flow of meteoric fluids—and likely the flow of other diagenetic fluids—while known to decrease CAS concentrations, have little effect on  $\delta^{34}\text{S}_{\text{CAS}}$  values (Gill et al., 2008; Sim et al., 2015; Lau and Hardisty, 2022). There is a weak correlation between  $\delta^{18}\text{O}_{\text{carb}}$  and [CAS] in the Mušlovka Quarry section, with  $R^2 = 0.21$  (Fig. 7D). However, it should be noted that most of the [CAS] are below 100 ppm, suggesting significant diagenetic alteration. Correlations between  $\delta^{13}\text{C}_{\text{carb}}$  &  $\delta^{34}\text{S}_{\text{CAS}}$  and  $\delta^{18}\text{O}_{\text{carb}}$  &  $\delta^{34}\text{S}_{\text{CAS}}$  are of minor to perhaps moderate significance at the Mušlovka Quarry section, with an  $R^2$  values of 0.34 and 0.27, respectively (Fig. 7E, F). When assessed in relation to the Lau and Hardisty (2022) diagenetic models the  $\delta^{34}\text{S}_{\text{CAS}}$  data plots outside of the fields related to diagenetic activity. The effects of meteoric diagenesis are still seen in the relatively low isotopic values of  $\delta^{13}\text{C}_{\text{carb}}$  and  $\delta^{18}\text{O}_{\text{carb}}$ . As stated previously though, meteoric diagenesis has very little effect on  $\delta^{34}\text{S}_{\text{CAS}}$ , which plays out in the near-horizontal dashed brown lines in the  $\delta^{13}\text{C}_{\text{carb}}-\delta^{34}\text{S}_{\text{CAS}}$  and  $\delta^{18}\text{O}_{\text{carb}}-\delta^{34}\text{S}_{\text{CAS}}$  model space (Lau and Hardisty, 2022).

The  $\delta^{34}\text{S}_{\text{CAS}}$  values at the Mušlovka Quarry section are noticeably lower than what seem to be baseline Ludfordian seawater values of  $\sim +24\text{‰}$ . This is based on pre- and post-excursion baseline  $\delta^{34}\text{S}_{\text{CAS}}$  values from multiple sections on the southern Laurentian margin (Bowman et al., 2020). As such,  $\delta^{34}\text{S}_{\text{CAS}}$  values from the Mušlovka Quarry section that were isotopically lighter than a conservative value of  $+20\text{‰}$  (values between  $+11.7$  to  $+19.7\text{‰}$ ; see Supplemental Data Tables) were discarded as not being representative of primary Ludfordian seawater and most likely contaminated by the oxidation of sedimentary pyrite during laboratory CAS extraction. This is likely attributable to the ubiquitous presence of pyrite within the Mušlovka Quarry section. High pyrite concentrations such as these complicate the CAS laboratory extraction process; the higher the pyrite concentration, the more likely it is to be oxidized during the acidification of powdered carbonate samples (e.g., Present et al., 2015; Edwards et al., 2019; Richardson et al., 2019). A slight correlation ( $R^2 = 0.24$ ) between  $\delta^{34}\text{S}_{\text{CAS}}$  and  $\delta^{34}\text{S}_{\text{pyr}}$  shows that when pyrite-sulfur values were isotopically lighter, CAS values also tended to be lighter (see Supplemental Data Tables). Though, it is also possible that the variability in the Ludfordian  $\delta^{34}\text{S}_{\text{CAS}}$  values is due to regional heterogeneity in the seawater sulfate pool resulting from low seawater sulfate concentrations. Relatively low seawater sulfate concentrations have also been suggested to contribute to small offsets in excursion magnitudes and baseline values between  $\delta^{34}\text{S}_{\text{CAS}}$  datasets for the late Cambrian Steptoean positive carbon isotope excursion (SPICE, Gill et al., 2011b) and middle Silurian

Ireviken event (Young et al., 2019). Recent sulfur isotope mass balance modeling done by Zhang et al. (2022) also supports the possibility of low seawater sulfate concentrations during the Ludfordian. Based on their model results concentrations may have been as low as 1.1 – 1.2 mM in the late Silurian oceans (compared to 28 mM in the modern ocean; Zhang et al., 2022).

### **Local Redox of the Shallow Shelf**

I/Ca values were low (0 – 0.4  $\mu\text{mol/mol}$ ) throughout the Mušlovka Quarry section and showed no systematic variation between carbonate matrix and clasts within the flat-pebble conglomerate intervals (Fig. 4D). This could be the result of consistently low or no oxygen in the water column or adjacent water masses (e.g., Lu et al., 2010, 2018). I/Ca analyses typically target micritic matrix and in the case of Mušlovka Quarry, much of what was once micritic matrix has been heavily dolomitized, with even skeletal grains showing partial recrystallization (Fig. 3D, E). Importantly, the one I/Ca value notably above the detection limit ( $\sim 2.7 \mu\text{mol/mol}$ ) is stratigraphically above the dolomitized interval. Given the complicated tectonic history (see Geologic Setting) and the clear signal of meteoric diagenesis (see Diagenesis Discussion) it is unlikely that the I/Ca values from Mušlovka are a primary seawater signature (Lau and Hardisty, 2022).

In the shallow tropical seas of both Laurentia and Baltica, notable positive excursions in  $\delta^{34}\text{S}_{\text{CAS}}$  have been documented, with magnitudes between +8 to +30‰, recording the enhanced burial and preservation of pyrite across the global oceans (Bowman et al., 2019, 2020). Again, in sections from Laurentia and Baltica this is accompanied by parallel positive excursions in  $\delta^{34}\text{S}_{\text{pyr}}$ , with magnitudes between +20 to +68‰, which mirror this signal of enhanced pyrite burial on a local to regional scale. At the Mušlovka Quarry there was no positive excursion recorded to suggest that the record of  $\delta^{34}\text{S}_{\text{pyr}}$  is reflective of the global changes in sulfur isotopes of seawater sulfate that have been recorded on the southern Laurentian margin and in the Baltic Basin (Bowman et al., 2019, 2020). Thus, it is likely that the  $\delta^{34}\text{S}_{\text{pyr}}$  values were representative of local factors such as rate of microbial sulfate reduction (MSR), sulfate concentrations, the availability of organic matter or iron, changes in the location of pyrite formation, changes in sedimentation rates, and/or changes in sea level (e.g., Canfield and Thamdrup, 1994; Leavitt et al., 2013; Gomes and Hurtgen, 2015; Kozłowski, 2015; Farkaš et al., 2016; Sim, 2019; Pasquier et al., 2021).

The isotopic difference ( $\Delta^{34}\text{S}$ ) between marine sulfate ( $\delta^{34}\text{S}_{\text{CAS}}$ ) and sedimentary pyrite ( $\delta^{34}\text{S}_{\text{pyr}}$ ) can be indicative of locus of pyrite formation in the water column and/or sediment porewaters and its formation via open- or closed-system MSR (Gomes and Hurtgen, 2015). Based on limited  $\delta^{34}\text{S}_{\text{CAS}}$  data at Mušlovka Quarry (Fig. 4B), lower  $\Delta^{34}\text{S}$  values of  $\sim 24\text{‰}$  (due to higher  $\delta^{34}\text{S}_{\text{pyr}}$ ) in the lower part of the section, the *N. inexpectatus* zone, could be indicative of pyrite formation via more closed-system MSR within sediment porewaters. Higher  $\Delta^{34}\text{S}$  values of 35 to 50‰ in the upper part of the section (*M. fragmentalis* zone) imply that pyrite formed via more open-system MSR, either in the water column or at the sediment-water interface (Gomes and Hurtgen, 2015). Though our  $\delta^{34}\text{S}_{\text{pyr}}$  data is not reflective of the global enhancement of pyrite burial during the mid-Ludfordian, pyrite concentrations in the Mušlovka Quarry carbonate succession were high throughout the section, with sedimentary pyrite being observed in both hand sample and thin section (Fig. 4C). Pyrite concentrations averaged  $\sim 600$  ppm and were as high as 1200 ppm in the upper part of the section (Fig. 3C). Thus, suggesting at the very least that sediment porewaters in the shallow shelf of the Prague Basin were reducing and likely sulfidic (Fig. 9). The low I/Ca values, prevalence of finely disseminated pyrite through the measured section, and high  $\Delta^{34}\text{S}$  values all support the possibility of reducing bottom-water and sediment porewater conditions at the site of the shallow shelf deposition of the Mušlovka Quarry section.

### Local Redox of the Deep Shelf

The iron speciation and trace element concentrations from mid-Ludfordian successions have been documented previously in the deep shelf shales and mudstones of the tropical Baltic Basin and Richardson Trough (Bowman et al. 2021; Sperling et al., 2021) and the mid-latitudes of Peri-Gondwana (Frýda et al., 2021b). At Kosov Quarry, in the deep shelf section of the Prague Basin, the ratios of highly reactive to total iron ( $\text{Fe}_{\text{HR}}/\text{Fe}_{\text{T}}$ ) of the shale interbeds were almost all greater than 0.38, consistent with values associated with modern marine sediments deposited under anoxic water column conditions (Fig. 6A). Only 4 samples, all in the *N. kozłowski* zone, fell within the 0.22 to 0.38 range, representing possibly anoxic or fluctuating redox conditions in the water column (Poulton and Canfield, 2005; Raiswell et al., 2018). Pyrite to highly reactive iron ( $\text{Fe}_{\text{pyr}}/\text{Fe}_{\text{HR}}$ ) values plot almost entirely within the ferruginous field ( $< 0.7$ ), with only 4 samples plotting as possibly euxinic to euxinic within the LKE interval (Fig. 6B). This new iron speciation data suggest that local bottom waters were reducing before, during, and after this global marine extinction event (Fig. 9) but sulfide was likely limited with relatively little formation of pyrite from reactive iron minerals. These

trends are consistent with previously published iron speciation data from the Priekule-20 drill core deposited in the deep shelf of the Baltic Basin that show a local pulse of sulfidic sediment porewater conditions during the same approximate stratigraphic interval during the LKE event (Bowman et al., 2021). Similarly, samples from the Richardson Trough in the Yukon of northwest Canada indicate that anoxic areas of the late Silurian ocean were ferruginous, but likely not euxinic, through the LKE and Lau CIE on the northern margin of Laurentia (Sperling et al., 2021).  $Fe_T/Al$  ratios were somewhat variable through the Kosov Quarry section, between 0.47 – 0.87 (Fig. 6C). These values are compared to the average for Paleozoic oxic marine shales of  $0.53 \pm 0.11$  (Raiswell et al., 2018).  $Fe_T/Al$  values above 0.64 are typically indicative of benthic iron shuttling within a basin (e.g., Raiswell et al., 2018). The  $Fe_T/Al$  ratios average 0.64, with most values above the Paleozoic average, indicating the likelihood of some benthic iron shuttling from shallow to deep shelf sediments in the Prague Basin during the Ludfordian. These values could suggest a variation in locus of reducing conditions throughout the Ludfordian in the deep shelf of the Prague Basin, with the iron reduction zone moving back and forth across the sediment-water interface (Fig. 9; Hardisty et al., 2018; Raiswell et al., 2018).

As mentioned previously, the reported trace metal concentrations discussed below have been corrected for variable lithological changes such as carbonate content and then, for all trace metals aside from Mn, normalized with total organic carbon content from each sample. Mn concentrations recorded from the Kosov Quarry section average ~ 175 ppm throughout the section with no notable trends, well below the average of 850 ppm for modern oxic sediments (Fig. 6D; Morford and Emerson, 1999). There are a few data points with relatively high values in the *P. dubius postfrequens* and *M. latilobus* – *S. balticus* graptolite zones, but even these are still well below the modern oxic sediment average. These [Mn] data are indicative of bottom waters that were suboxic to anoxic, preventing the longterm burial of Mn-oxides. This is consistent with the independent findings of the Fe speciation proxy suggesting consistent locally anoxic water column conditions (Fig. 9).

Vanadium requires local suboxic to anoxic water column conditions to become enriched within sediments, but not necessarily euxinic conditions (Algeo and Maynard, 2004; Owens et al., 2016, 2017). Total organic carbon normalized vanadium concentrations in the Kosov Quarry are moderately enriched in the *N. inexpectatus* and *N. kozlowskii* zones, averaging ~340 ppm/wt%, and decrease through the LKE interval to ~157 ppm/wt% (Fig. 6E). The moderate V/TOC enrichments throughout the section are consistent with locally suboxic-

anoxic water columns. Trends between the carbonate corrected and TOC normalized [V] are similar, highlighting the possibility of a shift in the global V reservoir rather than the local influence of variable organic matter deposition in the Prague Basin (Algeo and Rowe, 2012). The trend in V/TOC from higher to lower values moving upward throughout the section could indicate a trend from anoxic to more suboxic or fluctuating redox conditions, although there was no corresponding change in Fe speciation data to support this. Alternatively, this trend towards lower [V] might be reflective of changes in the global inventory of vanadium in the late Silurian oceans (see discussion of Global Redox below).

Total organic carbon normalized uranium concentrations range from ~10 to 150 ppm/wt% in the Kosov Quarry section (Fig. 6F). The accumulation of U in sediments is reliant on the diffusion of uranyl-carbonate ions and the reduction from  $U^{6+}$  to  $U^{4+}$  across the sediment-water interface; thus, enriched U concentrations indicate anoxic bottom water conditions (Tribovillard et al., 2006). Across the upper boundary of the *N. kozłowskii* biozone average U/TOC decreases slightly from 73 to 66 ppm/wt%. Overall, the U/TOC data suggest relatively consistent bottom water anoxia through the Ludfordian, in agreement with the Fe speciation and [Mn] data (Fig. 9).

Mild enrichments in molybdenum were also preserved in the Kosov Quarry section. Mo requires euxinic conditions to significantly enrich in sediments and is often associated with the burial of organic carbon (Fig. 6G). Mo/TOC averaged ~23 ppm/wt% and, taken together with the Fe speciation data, suggests predominantly anoxic water column conditions with possibly sulfidic sediment porewaters (Fig. 9; Hardisty et al., 2018). As with V and U there is a notable decrease in Mo/TOC across the upper boundary of the *N. kozłowskii* zone from an average of ~27 to ~20 ppm/wt%. The Mo/TOC values at Kosov Quarry are similar to those of the modern-day silled Cariaco Basin (Fig. 9; Algeo and Lyons, 2006) and could suggest some minor amount of hydrographic restriction for the Prague Basin as suggested by Frýda et al. (2021b) but certainly points to a continued connection with the open ocean to allow for such elevated enrichments.

The trends in the TOC normalized concentrations of V, U, and Mo from the shale interbeds of Kosov Quarry in this study correspond well to those published by Frýda et al. (2021b) from both the shale and carbonate interbeds (cf., their Fig. 6 to Fig. 6E–G this study) and similar data in the same time interval from the deep shelf of the Baltic Basin published by Bowman et al. (2021). The decreases in redox-sensitive trace element concentrations during

the Lau CIE and after the LKE event are even more notable in the data from Frýda et al. (2021b), as they have higher sampling density from the inclusion of the limestone and marl interbeds in the geochemical analyses.

Based on the calculated values for uranium and molybdenum enrichment factors, both trace elements show substantial enrichment throughout the shales of the Kosov Quarry, with almost all  $U_{EF}$  and  $Mo_{EF}$  values greater than 10 (Algeo and Tribovillard, 2009). This further supports that local marine redox conditions were reducing throughout the Ludfordian (Fig. 9). Generally higher  $U_{EF}$  values than  $Mo_{EF}$  values, averages of 22 and 16 respectively, imply that suboxic to anoxic conditions were dominant as opposed to euxinic conditions. This indicates that the iron reduction zone was likely at or near the sediment-water interface allowing for the additional enrichment of U and bolsters the interpretations of local redox conditions from the Fe speciation data (Morford and Emerson, 1999; Algeo and Tribovillard, 2009). Cross plots of  $U_{EF}$  and  $Mo_{EF}$  can be used to interpret basin connectivity, as well, based on the comparison of Mo/U molar ratios to that of open ocean seawater values ( $\sim 7.5 - 7.9$ ; Algeo and Tribovillard, 2009). These ratios are shown as parallel lines on  $U_{EF}$  and  $Mo_{EF}$  cross plots (Fig. 8). Mo/U ratios for the Kosov Quarry shale interbeds fall primarily between 0.1 to 0.3 times the molar ratio of sea water, this indicates the samples were likely deposited either under fluctuating redox conditions or in a restricted basin (Fig. 8, blue symbols; Algeo and Tribovillard, 2009). The presence of cosmopolitan conodont and graptolite fauna throughout both the Mušlovka and Kosov Quarry sections requires a strong connection to the open ocean and prohibits the possibility of complete restriction (Havlíček and Štorch, 1990; Kříž, 1991, 1992; Manda, 2008). This provides further evidence that the Kosov Quarry shales were deposited in a silled marine basin as previously suggested due to the active Silurian faulting and volcanic activity in the region (e.g., Tasáryová et al., 2018). Slight hydrographic restriction due to a marine sill in the Prague Basin may help explain the coincidence of low Mo/U with cosmopolitan marine fauna (Fig. 9).

Frýda et al. (2021b) also published Mo/U molar ratios from the Kosov Quarry. Their  $U_{EF}$  and  $Mo_{EF}$  data, which includes samples from the limestone and marl interbeds, has a much wider spread, ranging from 0.1 to 1.0 times the molar ratio of seawater (Fig. 8, pink & green symbols). The larger range in their  $U_{EF}$  and  $Mo_{EF}$  data could reflect variation in the specific part of the shelf the sediments were formed in, with sediments initially recording the local marine redox conditions in those (shallower) locations and then subsequently transported to this deep shelf setting. Specifically, this deep shelf setting is comprised of alternating beds of

shale and carbonate lithologies, with the carbonates interpreted to be tempestites (i.e., storm deposits from the nearby shallow carbonate bank) and not formed *in situ* but transported some distance (Manda et al., 2012; Gocke et al., 2013). Consequently, the interbeds of shale/mudstone should record the ‘background’ sedimentation and therefore local marine redox conditions more representative of the Kosov Quarry deep shelf environment. Thus, the overall higher degree of variability in the  $U_{EF}$  and  $MO_{EF}$  data of Frýda et al. (2021a) may reflect the variation in strata that is representative of background sedimentation at Kosov Quarry as well as being reflective of other shallower marine environments nearby (e.g., the use of both carbonates and mudstone/shales). Alternatively, their data may track the evolution of water mass chemistry due to the interplay of global and local sea level change within the Prague Basin. During the Ludfordian, sea level has been inferred from sequence stratigraphic models to be the lowest during the Lau CIE, during the mid-Ludfordian glaciation, with relatively high sea level pre- and post-CIE (e.g., Lehnert et al., 2007; Eriksson and Calner, 2008; Frýda et al., 2021b). Prior to the Lau CIE (Fig. 8, pink symbols; Frýda et al., 2021a) during times of globally higher sea level, there were overall higher authigenic enrichments of redox-sensitive trace metals suggesting that the Prague Basin was well-connected to the Rheic Ocean. For some of the Frýda et al. (2021) pre-excursion data,  $MO_{EF} > U_{EF}$  (higher Mo/U) which may be related to the enrichment of Mo in sulfidic porewaters within nearby shallow carbonate sediments washed in as tempestite beds (Fig. 9). During the Lau CIE (Interval II, see Frýda et al., 2021a, b) authigenic enrichments were lower within the carbonate interbeds at a time when global sea level was at its lowest (Fig. 9B). Low authigenic enrichments and low Mo/U during this global sea level low are analogous to the record of enrichments and Mo/U along the basin margins of the Black Sea (Algeo and Tribovillard, 2009). This implies the sediments of the carbonate tempestite beds may have formed under an oxic water column in the mixed zone of the shallow shelf before being transported and deposited at the relatively deeper Kosov Quarry location. When combined with the relatively consistent Mo/U (~0.2 – 0.3) and high authigenic enrichment data from the shale interbeds this data is even more comparable to that of the Black Sea and may further suggest that the Prague Basin was silled (Fig. 9).

The bulk of the  $\delta^{34}S_{pyr}$  data documented at the Kosov Quarry most likely reflect global changes in pyrite burial and euxinia and are discussed below (see Global Redox section), here we discuss trends and excursions in the  $\delta^{34}S_{pyr}$  data that are more likely related to local factors. The large degree of scatter in the  $\delta^{34}S_{pyr}$  data in the lower part of the section within

the *N. inexpectatus* zone is likely a result of changes in local factors affecting MSR such as the location of pyrite formation—in either the water column or sediment pore waters—or variations in the availability of sulfate for MSR and/or reactive iron for the formation of pyrite. Post-CIE, in the *M. latilobus* – *S. balticus* and *M. fragmentalis* zones, there is an apparent second positive excursion in  $\delta^{34}\text{S}_{\text{pyr}}$  of more than 30‰. Frýda et al. (2021a) interpret this as a continuation of the main  $\delta^{34}\text{S}_{\text{pyr}}$  excursion that was interrupted with a negative isotope excursion in the lower-middle *M. latilobus*-*S. balticus* zone that resulted from an influx of isotopically negative sulfate from the open ocean during a transgression to temporarily fuel the production of hydrogen sulfide via MSR. Frýda et al. (2021b) noted that occurrence of new faunal communities at this stratigraphic level supports a hypothesis on a temporary influx of better-oxygenated ocean waters into a partly restricted epeiric basin as driver for rapid decrease of  $\delta^{34}\text{S}_{\text{pyr}}$  signal. Though there is no corresponding increase in pyrite concentrations documented at Kosov Quarry at that time (Frýda et al., 2021b). The delayed return to baseline values of  $\delta^{34}\text{S}$  relative to  $\delta^{13}\text{C}$  in the Lau CIE has been recorded in several other Ludfordian sections from Laurentia and Baltica (Bowman et al., 2020, 2021) though it is not clear if that is the cause of the apparently additional  $\delta^{34}\text{S}_{\text{pyr}}$  excursion seen here. The offset between these two stable isotope records may be linked to a continuation of enhanced pyrite burial rates due to the accumulation of labile organic matter (i.e., Lau CIE-related  $\text{C}_{\text{org}}$  burial) on the seafloor and within the upper parts of marine sediments.

### Implications for Ludfordian Global Redox Changes

The parallel  $\delta^{13}\text{C}_{\text{carb}}$  and  $\delta^{34}\text{S}_{\text{pyr}}$  excursions recorded from this locally anoxic marine setting in the Prague Basin (Frýda et al., 2021b, and this study), when combined with stable isotopic records from other paleocontinents (e.g.,  $\delta^{34}\text{S}_{\text{CAS}}$ ), suggest major changes in global marine redox conditions occurred during this interval of the late Silurian. These positive carbon and sulfur isotopic excursions imply enhanced burial of reduced carbon and sulfur as organic matter, pyrite, and organic sulfur compounds (Gill et al., 2011a; Owens et al., 2013). The high magnitude sulfur isotope excursion recorded both in sedimentary pyrite from our shale interbed samples (+30‰ in  $\delta^{34}\text{S}_{\text{pyr}}$ ; Fig. 5B, red symbols) and the sedimentary pyrite from marl and limestone samples (+20‰ in  $\delta^{34}\text{S}_{\text{pyr}}$ ; Fig. 5B, blue symbols) recently published by Frýda et al. (2021a, b) from the Kosov Quarry section correlate with the +20 to +68‰ magnitude  $\delta^{34}\text{S}_{\text{pyr}}$  excursions documented in Baltica (Bowman et al., 2019, 2021) and in southern Laurentia (Bowman et al., 2020) during the LKE and Lau CIE interval. The positive excursion in  $\delta^{34}\text{S}_{\text{CAS}}$  records from shallow shelf carbonates of the Baltic Basin (+30‰), the

southern margin of Laurentia (+8‰) and deeper shelf of the Peri-Gondwana (+15‰) indicate that there was not only an expansion of anoxia in the mid-Ludfordian (Fig. 9), but also an enhanced pyrite burial on many continental margin settings at this time due to expanded euxinic bottom water conditions (Bowman et al., 2019, 2020; Frýda et al. 2021a, b). A recent study of  $\delta^{238}\text{U}$  records (del Rey *et al.* 2023) from temperate (Kosov, peri-Gondwana) and tropical (Broken River, eastern Gondwana) settings also support previous findings (Bowman et al., 2019; Frýda et al. 2021b) that reducing conditions expanded in the global oceans before and during the onset of the Lau CIE, and was contemporaneous with the faunal extinctions during the Lau/Kozlowskii extinction event.

The onset of the positive excursion in the  $\delta^{34}\text{S}_{\text{pyr}}$  from Kosov Quarry occurs stratigraphically higher (after) the onset of the Lau CIE in both our dataset and the Frýda et al. (2021a) dataset. This offset pattern in  $\delta^{34}\text{S}$  relative to  $\delta^{13}\text{C}$  at Kosov Quarry is consistent with previously published paired C and S records from other paleocontinents and supports the hypothesis that in the mid-Ludfordian enhanced organic carbon burial pre-dated increased pyrite burial and expansion of euxinic conditions (Bowman et al., 2020, 2021; Frýda et al. 2021b).

Although the trends in trace elements in the Kosov Quarry have been interpreted above to represent changes in local redox conditions, inferences can be drawn about global redox changes when these data are considered within the context of time correlative local and global marine redox proxy data from other paleo-ocean basins (i.e., Bowman et al., 2019, 2020, 2021; Frýda et al. 2021a, b). In the Kosov Quarry section, trace metal concentrations decrease from the *N. kozlowskii* through the *P. dubius postfrequens* coincident with the positive excursion of  $\delta^{34}\text{S}_{\text{pyr}}$  and  $\delta^{34}\text{S}_{\text{CAS}}$  that is linked to the expansion of euxinic conditions globally. Reducing sediments more readily sequester trace metals as anoxic to euxinic conditions expand along continental margins throughout global oceans (Owens et al., 2016). A drop in trace metal concentrations (V, Hg, U, Mo) during this same approximate time interval is also recorded in the Priekule-20 core from Latvia (Baltic Basin; Bowman et al., 2021) and trace metal datasets previously reported from marl and limestone interbeds from Kosov Quarry (Frýda et al., 2021b). Collectively these data suggest bottom water deoxygenation may have led to global trace metal drawdown during the Lau CIE (e.g., Owens et al., 2016; Frýda et al., 2021b). Ultimately, additional Ludfordian trace metal records from globally dispersed localities are needed from shale successions that are persistently euxinic throughout this time interval to definitively test this hypothesis.

## Conclusions

We have presented new geochemical redox proxy data from the shallow shelf carbonates of the Mušlovka Quarry section and the shale interbeds from the deeper shelf section at Kosov Quarry, both from the Prague Basin of the mid-latitude peri-Gondwanan Barrandian Terrane. Initial microfacies analysis of the Mušlovka Quarry section show that diagenetic processes notably affected primary carbonate textures through dolomitization, recrystallization, and common secondary calcite veins and euhedral pyrite. There are no significant stratigraphic trends in the I/Ca and  $\delta^{34}\text{S}_{\text{pyr}}$  records from Mušlovka Quarry. The low I/Ca values throughout the Mušlovka Quarry section could be reflective of either consistent local anoxic waters nearby or diagenetic overprinting during the complex tectonic and burial history of this region. However, elevated pyrite concentrations indicate that the local marine environment was most likely reducing in the sediment porewaters at the very least. The  $\delta^{34}\text{S}_{\text{pyr}}$  values at Mušlovka Quarry appear to reflect local sulfur cycling within the likely sulfidic sediment porewaters. Due to the high pyrite contents of the Mušlovka Quarry carbonates the majority of our  $\delta^{34}\text{S}_{\text{CAS}}$  data presented here are consistent with contamination via pyrite oxidation during the chemical extraction process for carbonate-associated sulfate.

In the Kosov Quarry iron speciation data suggests a locally anoxic marine water column throughout the sampled succession, with intervals of benthic iron shuttling. Consistently low concentrations of Mn support the interpretation of water column anoxia, and particularly bottom-water anoxia which would have prevented the accumulation of Mn-oxides. Enrichments in redox-sensitive trace elements throughout the section were also consistent with local anoxia. The excursion in  $\delta^{34}\text{S}_{\text{pyr}}$  values from Kosov Quarry coincident with the Lau CIE suggests increased reduced carbon and sulfur burial as organic matter and pyrite (Gill et al., 2011a; Owens et al., 2013). The trends in the  $\delta^{34}\text{S}_{\text{pyr}}$  data from Kosov Quarry likely reflect the global enhancement of pyrite burial and euxinia in the Ludfordian oceans. Notable drawdowns in redox-sensitive trace elements (V, U, Mo) in the same stratigraphic interval from two hydrographically separated and geographically disparate ocean basins further support the severity and global nature of the marine redox changes associated with the LKE (Laurentia, Tennessee Shelf: Bowman et al., 2020; Baltic Basin: Bowman et al., 2021; Prague Basin: this study; Frýda et al., 2021b). Though, more work is needed from Ludfordian

sections with evidence of persistent local euxinia to better test this trace metal drawdown hypothesis.

This multiproxy, multi-lithology investigation gives a holistic perspective on local and global redox changes in the late Silurian oceans. Expanded marine anoxia and/or euxinia provides a plausible mechanism for the Lau/Kozlowskii extinction as deoxygenated waters containing appreciable free hydrogen sulfide would have induced significant stress on marine life (e.g., Meyer and Kump, 2008). The extent and severity of the expansive reducing conditions during the Lau CIE and LKE has become much clearer, despite the complications and complexities inherent to unravelling ancient local and global marine redox conditions.

## **Acknowledgements**

We thank Sean Newby for assistance in sample processing and data collection. We thank two anonymous reviewers and Editor Simon Poulton for their detailed and constructive feedback which helped to improve this paper.

## **Author Contributions**

[will be automatically generated based on info provided in submission process]

## **Funding**

This research was funded by the National Science Foundation (EAR-1748635 to SAY and JDO) and by the Grant Agency of the Czech Republic (GA23-06198S to JF). This research was performed at the National High Magnetic Field Laboratory, which is supported by NSF Cooperative Agreement No. DMR-1644770 and the State of Florida.

## **Data Availability Statement**

The datasets used for this article are available in the supplementary material.

## References

- Algeo, T.J. and Lyons, T.W. 2006. Mo-total organic carbon covariation in modern anoxic marine environments: Implications for analysis of paleoredox and paleohydrographic conditions. *Paleoceanography*, **21**, PA1016. <https://doi.org/10.1029/2004PA001112>
- Algeo, T.J. and Maynard, J.B. 2004. Trace-element behavior and redox facies in core shales of Upper Pennsylvanian Kansas-type cyclothems. *Chemical Geology*, **206**, 289-318. <https://doi.org/10.1016/j.chemgeo.2003.12.009>
- Algeo, T.J. and Rowe, H. 2012. Paleoceanographic applications of trace-metal concentration data. *Chemical Geology*, **324-325**, 6-18. <https://doi.org/10.1016/j.chemgeo.2011.09.002>
- Algeo, T.J. and Tribovillard, N. 2009. Environmental analysis of paleoceanographic systems based on molybdenum-uranium covariation. *Chemical Geology*, **268**, 211-225. <https://doi.org/10.1016/j.chemgeo.2009.09.001>
- Banner, J.L. and Hanson, G.N. 1990. Calculation of simultaneous isotopic and trace element variations during water-rock interaction with applications to carbonate diagenesis. *Geochimica et Cosmochimica Acta*, **54**, 3123-3137. [https://doi.org/10.1016/0016-7037\(90\)90128-8](https://doi.org/10.1016/0016-7037(90)90128-8)
- Bickert, T., Patzold, J., Samtleben, C. and Munnecke, A. 1997. Paleoenvironmental changes in the Silurian indicated by stable isotopes in brachiopod shells from Gotland, Sweden. *Geochimica et Cosmochimica Acta*, **61**, 2717-2730. [https://doi.org/10.1016/S0016-7037\(97\)00136-1](https://doi.org/10.1016/S0016-7037(97)00136-1)
- Bond, D.P.G. and Grasby, S.E. 2017. On the causes of mass extinctions. *Palaeogeography Palaeoclimatology Palaeoecology*, **478**, 3-29. <https://doi.org/10.1016/j.palaeo.2016.11.005>
- Bowman, C.N., Lindskog, A., Kozik, N.P., Richbourg, C.G., Owens, J.D. and Young, S.A. 2020. Integrated sedimentary, biotic, and paleoredox dynamics from multiple localities in southern Laurentia during the late Silurian (Ludfordian) extinction event. *Palaeogeography Palaeoclimatology Palaeoecology*, **553**, 109799. <https://doi.org/10.1016/j.palaeo.2020.109799>
- Bowman, C.N., Them II, T.R., Knight, M.D., Kaljo, D., Eriksson, M.E., Hints, O., Martma, T., Owens, J.D. and Young, S.A. 2021. A multi-proxy approach to constrain reducing

conditions in the Baltic Basin during the late Silurian Lau carbon isotope excursion.

*Palaeogeography Palaeoclimatology Palaeoecology*, **581**, 110624.

<https://doi.org/10.1016/j.palaeo.2021.110624>

Bowman, C.N., Young, S.A., Kaljo, D., Eriksson, M.E., Them II, T.R., Hints, O., Martma, M. and Owens, J.D. 2019. Linking the progressive expansion of reducing conditions to a stepwise mass extinction event in the late Silurian oceans. *Geology*, **47**, 968-972.

<https://doi.org/10.1130/G46571.1>

Brüchert, V. and Pratt, L.M. 1996. Contemporaneous early diagenetic formation of organic and inorganic sulfur in estuarine sediments from St. Andrew Bay, Florida, USA. *Geochimica et Cosmochimica Acta*, **60**, 2325-2332. [https://doi.org/10.1016/0016-7037\(96\)00087-7](https://doi.org/10.1016/0016-7037(96)00087-7)

Calner, M. 2008. Silurian global events — at the tipping point of climate change. In: *Mass extinctions* (Eds A.M.T. Elewa) pp. 21-58. Springer-Verlag, Berlin Heidelberg.

[https://doi.org/10.1007/978-3-540-75916-4\\_4](https://doi.org/10.1007/978-3-540-75916-4_4)

Canfield, D.E., Raiswell, R., Westrich, J.T., Reaves, C.M. and Berner, R.A. 1986. The use of chromium reduction in the analysis of reduced inorganic sulfur in sediments and shales.

*Chemical Geology*, **54**, 149-155. [https://doi.org/10.1016/0009-2541\(86\)90078-1](https://doi.org/10.1016/0009-2541(86)90078-1)

Canfield, D.E. and Thamdrup, B. 1994. The production of  $^{34}\text{S}$ -depleted sulfide during bacterial disproportionation of elemental sulfur. *Science*, **266**, 1973-1975.

<https://doi.org/10.1126/science.11540246>

Chadimova, L., Vacek, F., Sobien, K., Slavik, L. and Hladil, J. 2015. Petrophysical record of the Late Silurian shallow-water carbonate facies across the Lau Event (Prague Synform, Czech Republic) and dynamic time warping alignment of the magnetic susceptibility logs.

*Geological Society of London, Special Publication*, **414**, 133-155.

<http://doi.org/10.1144/SP414.14>

Cocks, L.R.M. and Torsvik, T.H. 2002. Earth geography from 500 to 400 million years ago: a faunal and paleomagnetic review. *Journal of the Geological Society, London*, **159**, 631-644.

<https://doi.org/10.1144/0016-764901-118>

Cramer, B.D. and Saltzman, M.R. 2005. Sequestration of  $^{12}\text{C}$  in the deep ocean during the early Wenlock (Silurian) positive carbon isotope excursion. *Palaeogeography*

*Palaeoclimatology Palaeoecology*, **219**, 333-349.

<https://doi.org/10.1016/j.palaeo.2005.01.009>

Cramer, B.D. and Saltzman, M.R. 2007. Fluctuations in epeiric sea carbonate production during Silurian positive carbon isotope excursions: A review of proposed paleoceanographic models. *Palaeogeography Palaeoclimatology Palaeoecology*, **245**, 37-45.

<https://doi.org/10.1016/j.palaeo.2006.02.027>

Crampton, J.S., Cooper, R.A., Sadler, P.M. and Foote, M. 2016. Greenhouse—icehouse transition in the Late Ordovician marks a step change in extinction regime in the marine plankton. *Proceedings of the National Academy of Sciences, United States of America*, **113**, 1498-1503. <https://doi.org/10.1073/pnas.1519092113>

del Rey, A., Havsteen, J.C., Bizarro, M. and Dahl, T.W. 2020. Untangling the diagenetic history of uranium isotopes in marine carbonates: A case study tracing the  $\delta^{238}\text{U}$  composition of late Silurian oceans using calcitic brachiopod shells. *Geochimica et Cosmochimica Acta*, **287**, 93-110. <https://doi.org/10.1016/j.gca.2020.06.002>

del Rey, Á., Frýda, J., Calner, M., Frýdová, B., Zhang, F., Wang, Ch., Planavsky, N. and Dahl, T.W. 2023. Mid-Ludfordian uranium isotope records distinguish the role of expansive marine anoxia in global carbon cycle dynamics during the late Silurian Lau/Kozlowski bioevent. *Planetary and Global Change*, **229**, 1-9, 104248.

<https://doi.org/10.1016/j.gloplacha.2023.104248>.

Edwards, C.T., Fike, D.A. and Saltzman, M.R. 2019. Testing carbonate-associated sulfate (CAS) extraction methods for sulfur isotope stratigraphy: A case study of a Lower-Middle Ordovician carbonate succession, Shingle Pass, Nevada, USA. *Chemical Geology*, **529**, 119297. <https://doi.org/10.1016/j.chemgeo.2019.119297>

Epstein, A.G., Epstein, J.B. and Harris, L.D. 1977. Conodont color alteration — an index to organic metamorphism. *United States Geological Survey Professional Paper*, **995**, 1-27.

<https://doi.org/10.3133/pp995>

Eriksson, M.E., Nilsson, E.K. and Jeppsson, L. 2009. Vertebrate extinctions and reorganizations during the Late Silurian Lau Event. *Geology*, **37**, 739-742.

<https://doi.org/10.1130/G25709A.1>

Eriksson, M.J. and Calner, M. 2008. A sequence stratigraphical model for the late Ludfordian (Silurian) of Gotland, Sweden: implications for timing between changes in sea level, palaeoecology, and global carbon cycle. *Facies*, **54**, 253-276. <http://doi.org/10.1007/s10347-007-0128-y>

Farkaš, J., Frýda, J. and Holmden, C. 2016. Calcium isotope constraints on the marine carbon cycle and CaCO<sub>3</sub> deposition during the late Silurian positive  $\delta^{13}\text{C}$  excursion. *Earth and Planetary Science Letters*, **451**, 31–40. <https://doi.org/10.1016/j.epsl.2016.06.038>

Ferretti, A. and Kříž, J. 1995. Cephalopod Limestone Biofacies in the Silurian of the Prague Basin, Bohemia. *Palaios*, **10**, 240-253. <https://doi.org/10.2307/3515255>

Frýda, J. and Manda, Š. 2013. A long-lasting steady period of isotopically heavy carbon in the late Silurian ocean: evolution of the  $\delta^{13}\text{C}$  record and its significance for an integrated  $\delta^{13}\text{C}$ , graptolite and conodont stratigraphy. *Bulletin of Geosciences*, **88**, 463-482. <https://doi.org/10.3140/bull.geosci.1436>

Frýda, J., Lehnert, O., Frýdová, B., Farkaš, J. and Kubajko, M. 2021a. Carbon and sulfur cycling during the mid-Ludfordian anomaly and the linkage with the late Silurian Lau/Kozłowski Bioevent. *Palaeogeography Palaeoclimatology Palaeoecology*, **564**, 110152. <https://doi.org/10.1016/j.palaeo.2020.110152>

Frýda, J., Lehnert, O., Joachimski, M.M., Männik, P., Kubajko, M., Mergl, M., Farkas, J. and Frýdová, B. 2021b. The Mid-Ludfordian (late Silurian) Glaciation: A link with global changes in ocean chemistry and ecosystem overturns. *Earth-Science Reviews*, **220**, 103652. <https://doi.org/10.1016/j.earscirev.2021.103652>

Gill, B.C., Lyons, T.W. and Frank, T.D. 2008. Behavior of carbonate-associated sulfate during meteoric diagenesis and implications for the sulfur isotope paleoproxy. *Geochimica et Cosmochimica Acta*, **72**, 4699-4711. <https://doi.org/10.1016/j.gca.2008.07.001>

Gill, B.C., Lyons, T.W. and Jenkyns, H.C. 2011a. A global perturbation to the sulfur cycle during the Toarcian Oceanic Anoxic Event. *Earth and Planetary Science Letters*, **312**, 484-496. <https://doi.org/10.1016/j.epsl.2011.10.030>

Gill, B.C., Lyons, T.W., Young, S.A., Kump, L.R., Knoll, A.H. and Saltzman, M.R. 2011b. Geochemical evidence for widespread euxinia in the Later Cambrian ocean. *Nature*, **469**, 80-83. <https://doi.org/10.1038/nature09700>

Gocke, M., Lehnert, O. and Frýda, J. 2013. Facies development and palynomorphs during the Lau Event (Late Silurian) in a non-tropical carbonate environment: shallow and deep water examples from the Barrandian Area (Czech Republic). *Facies*, **59**, 611–630.

<http://doi.org/10.1007/s10347-012-0328-y>

Gomes, M.L. and Hurtgen, M.T. 2015. Sulfur isotope fractionation in modern euxinic systems: implications for paleoenvironmental reconstructions of paired sulfate-sulfide isotope records. *Geochimica et Cosmochimica Acta*, **157**, 39-55.

<https://doi.org/10.1016/j.gca.2015.02.031>

Hackley, P.C. and Cardott, B.J. 2016. Application of organic petrography in North American shale petroleum systems: A review. *International Journal of Coal Geology*, **163**, 8-51.

<https://doi.org/10.1016/j.coal.2016.06.010>

Hardisty, D.S., Lu, Z., Bekker, A., Diamond, C.W., Gill, B.C., Jiang, G., Kah, L.C., Knoll, A.H., Loyd, S.J., Osburn, M.R., Planavsky, N.J., Wang, C., Zhou, X. and Lyons, T.W. 2017. Perspectives on Proterozoic surface ocean redox from iodine contents in ancient and recent carbonate. *Earth and Planetary Science Letters*, **463**, 159-170.

<https://doi.org/10.1016/j.epsl.2017.01.032>

Hardisty, D.S., Lu, Z., Planavsky, N.J., Bekker, A., Philippot, P., Zhou, X. and Lyons, T.W. 2014. An iodine record of Paleoproterozoic surface ocean oxygenation. *Geology*, **42**, 619-622. <https://doi.org/10.1130/G35439.1>

Hardisty, D.S., Lyons, T.W., Riedinger, N., Isson, T.T., Owens, J.D., Aller, R.C., Rye, D.M., Planavsky, N.J., Reinhard, C.T., Gill, B.C., Masterson, A.L., Asael, D. and Johnston, D.T. 2018. An Evaluation of Sedimentary Molybdenum and Iron as Proxies for Pore Fluid Paleoredox Conditions. *American Journal of Science*, **318**, 527-556.

<https://doi.org/10.2475/05.2018.04>

Havlíček, V. and Štorch, P., 1990. Silurian brachiopods and benthic communities in the Prague Basin (Czechoslovakia). *Rozpravy Ústředního ústavu geologického*, **48**, 1–275.

Havlíček, V., Vaněk, J. and Fatka, O. 1994. Perunica microcontinent in the Ordovician (its position within the Mediterranean Province, series division, benthic and pelagic associations). *Sborník geologických věd, Paleontologie*, **46**, 23–56.

Hrubcová, P., Šroda, P., Grad, M., Geissler, W.H., Guterch, A., Vozár, J., Hegedus, E. and Sudetes 2003 Working Group 2010. From the Variscan to the Alpine Orogeny: crustal structure of the Bohemian Massif and the Western Carpathians in the light of the SUDETES 2003 seismic data. *Geophysical Journal International*, **183**, 611-633.

<https://doi.org/10.1111/j.1365-246X.2010.04766.x>

Hurtgen, M.T., Arthur, M.A., Suits, N.S. and Kaufman, A.J. 2002. The sulfur isotopic composition of Neoproterozoic seawater sulfate: implications for a snowball Earth? *Earth and Planetary Science Letters*, **203**, 413-429. [https://doi.org/10.1016/S0012-821X\(02\)00804-X](https://doi.org/10.1016/S0012-821X(02)00804-X)

Hu, Z. and Gao, S. 2008. Upper crustal abundances of trace elements: A revision and update. *Chemical Geology*, **253**, 205-221. <https://doi.org/10.1016/j.chemgeo.2008.05.010>

Jeppsson, L. 1990. An oceanic model for lithological and faunal changes tested on the Silurian record. *Journal of the Geological Society, London*, **147**, 663-674.

<https://doi.org/10.1144/gsjgs.147.4.0663>

Jeppsson, L. and Landing, E. 1998. Silurian oceanic events: summary of general characteristics. *New York State Museum Bulletin*, **491**, 239-257.

Jeppsson, L. 2005. Conodont-based revisions of the Late Ludfordian on Gotland, Sweden. *Geologiska Föreningens I Stockholm Förhandlingar*, **127**, 273-282.

<https://doi.org/10.1080/11035890501274273>

Jeppsson, L. and Aldridge, R.J. 2000. Ludlow (late Silurian) oceanic episodes and events. *Journal of the Geological Society, London*, **157**, 1137-1148.

<https://doi.org/10.1144/jgs.157.6.1137>

Jones, D.S. and Fike, D.A. 2013. Dynamic sulfur and carbon cycling through the end-Ordovician extinction revealed by paired sulfate-pyrite  $\delta^{34}\text{S}$ . *Earth and Planetary Science Letters*, **363**, 144-155. <https://doi.org/10.1016/j.epsl.2012.12.015>

Kaljo, D., Kiipli, T. and Martma, T. 1997. Carbon isotope event markers through the Wenlock-Pridoli sequence at Ohesaare (Estonia) and Priekule (Latvia). *Palaeogeography Palaeoclimatology Palaeoecology*, **132**, 211-223. [https://doi.org/10.1016/S0031-0182\(97\)00065-5](https://doi.org/10.1016/S0031-0182(97)00065-5)

Koren', T.N. 1993. Main event levels in the evolution of the Ludlow graptolites. *Geological Magazine*, **1**, 44-52. <https://doi.org/10.1017/S0016756811000847>

Kozłowski, W. 2015. Eolian dust influx and massive whittings during the Kozłowski/Lau Event: carbonate hypersaturation as a possible driver of the mid-Ludfordian carbon isotope excursion, *Bulletin of Geosciences Czech Geological Survey*, **90**, 807–840. <https://doi.org/10.3140/bull.geosci.1581>

Kříž, J. 1991. The Silurian of the Prague Basin (Bohemia): Tectonic, eustatic, and volcanic controls on facies and faunal development. *Special Papers in Palaeontology*, **44**, 179–204.

Kříž, J. 1992. Silurian Field Excursions: Prague Basin (Barrandian), Bohemia. *National Museum of Wales, Cardiff, Geological Series*, **13**, 111pp.

Kříž, J. 1999. Bivalvia dominated communities of Bohemian type from the Silurian and Lower Devonian carbonate facies. In: Boucot, A.J. and Lawson, J.D. (eds). *Final report, project Ecostratigraphy. Paleocommunities: A case study from the Silurian and Lower Devonian*, 225-248. Cambridge University Press. [https://doi.org/10.1016/S0016-6995\(95\)80062-X](https://doi.org/10.1016/S0016-6995(95)80062-X)

Kříž, J. 2008. *Algerina* gen. nov. (Bivalvia, Nepiomorphia) from the Silurian of the North Gondwana margin (Algeria), peri-Gondwanan Europe (France, Italy), Perunica (Prague Basin, Bohemia) and the Siberian Plate (Tajmyr Basin, Russia). *Bulletin of Geosciences Czech Geological Survey*, **83**, 79-84. <https://doi.org/10.3140/bull.geosci.2008.01.079>

Kříž, J. and Schönlaub, H.P. 1980. Stop 1. Daleje Valley, Mušlovka Quarry section. In: Chlupáč, I., Kříž, J., and Schönlaub, H.P (eds). *Field Trip E, ECOS II, Barrandian*, Abhandlungen der Geologischen Bundesanstalt, **35**, 147-180.

Lau, K.V. and Hardisty, D.S. 2022. Modeling the impacts of diagenesis on carbonate paleoredox proxies. *Geochimica et Cosmochimica Acta*, **337**, 123-139. <http://doi.org/10.1016/j.gca.2022.09.021>

Leavitt, W.D., Halevy, I., Bradley, A.S. and Johnston, D.T. (2013) Influence of sulfate reduction rates on the Phanerozoic sulfur isotope record. *The Proceedings of the National Academy of Sciences*, **110**, 11244-11249. <https://doi.org/10.1073/pnas.1218874110>

Lehnert, O., Frýda, J., Buggisch, W. and Manda, S. 2003. A first report of the Ludlovian Lau event from the Prague Basin (Barrandian, Czech Republic). In: Ortega, G. and Aceñolaza, G.F. (eds). *Proceedings of the 7<sup>th</sup> International Graptolite Conference and Field Meeting of the International Subcommission on Silurian Stratigraphy*. Instituto Superior de Correlación Geológica, **18**, 139-144.

Lehnert, O., Frýda, J., Buggisch, W., Munnecke, A., Nützel, A., Kříž, J. and Manda, S. 2007.  $\delta^{13}\text{C}$  records across the late Silurian Lau event: New data from middle palaeo-latitudes of northern peri-Gondwana (Prague Basin, Czech Republic). *Palaeogeography Palaeoclimatology Palaeoecology*, **245**, 227-244.  
<https://doi.org/10.1016/j.palaeo.2006.02.022>

Lohmann, K.C. 1988. Diagenetic systems and their application in studies of paleokarst. In: James, N.P. and Choquette, P.W. (eds). *Paleokarst*, 58-80. Springer-Verlag.  
[https://doi.org/10.1007/978-1-4612-3748-8\\_3](https://doi.org/10.1007/978-1-4612-3748-8_3)

Lu, W., Ridgwell, A., Thomas, E., Hardisty, D.S., Luo, G., Algeo, T.J., Saltzman, M.R., Gill, B.C., Shen, Y., Ling, H., Edwards, C.T., Whalen, M.T., Zhou, X., Gutchess, K.M., Jin, L., Rickaby, R.E.M., Jenkyns, H.C., Lyons, T.W., Lenton, T.M., Kump, L.R. and Lu, Z. 2018. Late inception of a resiliently oxygenated upper ocean. *Science*, **361**, 174-177.  
<https://doi.org/10.1126/science.aar5372>

Lu, W., Wörmde, S., Halverson, G.P., Zhou, X., Bekker, A., Rainbird, R.H., Hardisty, D.S., Lyons, T.W. and Lu, Z. 2017. Iodine proxy evidence for increased ocean oxygenation during the Bitter Springs Anomaly. *Geochemical Perspective Letters*, **5**, 53-57.  
<https://doi.org/10.7185/geochemlet.1746>

Lu, Z., Hoogakker, B.A.A., Hillenbrand, C.-D., Zhou, X., Thomas, E., Gutchess, K.M., Lu, W., Jones, L. and Rickaby, R.E.M. 2016. Oxygen depletion recorded in upper waters of the glacial Southern Ocean. *Nature Communications*, **7**, 1-8.  
<https://doi.org/10.1038/ncomms11146>

Lu, Z., Jenkyns, H.C. and Rickaby, R.E.M. 2010. Iodine to calcium ratios in marine carbonate as a paleoredoxproxy during oceanic anoxic events. *Geology*, **38**, 1107-1110.  
<https://doi.org/10.1130/G31145.1>

- Manda, Š. 2008. Palaeoecology and palaeogeographic relations of the Silurian phragmoceratids (Nautiloidea, Cephalopoda) of the Prague Basin (Bohemia). *Bulletin of Geosciences*, **83**, 39-62. <https://doi.org/10.3140/bull.geosci.2008.01.039>
- Manda, Š. and Frýda, J. 2014. Evolution of the late Ludlow to early Lochkovian brachiopod, trilobite and bivalve communities of the Prague Basin and their link with the global carbon cycle. *Geologiska Föreningens i Stockholm Förhandlingar*, **136**, 179–184. <https://doi.org/10.1080/11035897.2014.882404>
- Manda, Š. and Kříž, J. 2006. Environmental and biotic changes in subtropical isolated carbonate platforms during the Late Silurian Kozlowskii Event, Prague Basin. *Geologiska Föreningens i Stockholm Förhandlingar*, **128**, 161-168. <https://doi.org/10.1080/11035890601282161>
- Manda, Š., Štorch, P., Slavík, L., Frýda, J., Kříž, J. and Tasáryová, A. 2012. The graptolite, conodont and sedimentary record through the late Ludlow Kozlowskii Event (Silurian) in the shale-dominated succession of Bohemia. *Geological Magazine*, **149**, 507-531. <https://doi.org/10.1017/S0016756811000847>
- Marenco, P.J., Corsetti, F.A., Hammond, D.E., Kaufman, A.J. and Bottjer, D.J. 2008. Oxidation of pyrite during extraction of carbonate associated sulfate. *Chemical Geology*, **247**, 124-132. <https://doi.org/10.1016/j.chemgeo.2007.10.006>
- März, C., Poulton, S.W., Beckman, B., Küster, K., Wagner, T. and Kasten, S. 2008. Redox sensitivity of P cycling during marine black shale formation: Dynamics of sulfidic and anoxic, non-sulfidic bottom waters. *Geochimica et Cosmochimica Acta*, **72**, 3703-3717. <https://doi.org/10.1016/j.gca.2008.04.025>
- McAdams, N.E.B., Cramer, B.D., Bancroft, A.M., Melchin, M.J., Devera, J.A. and Day, J.E. 2019. Integrated  $\delta^{13}\text{C}_{\text{carb}}$ , conodont, and graptolite biogeochemistry of the Silurian from the Illinois Basin and stratigraphic revision of the Bainbridge Group. *Geological Society of America Bulletin*, **113**, 335-352. <https://doi.org/10.1130/B32033.1>
- McLennan, S.M. 2001. Relationships between the trace element composition of sedimentary rocks and upper continental crust. *Geochemistry Geophysics Geosystems*, **2**, 2000GC000109. <https://doi.org/10.1029/2000GC000109>

Mergl, M., Frýda, J., Kubajko, M. 2018. Response of organophosphatic brachiopods to the mid-Ludfordian (late Silurian) carbon isotope excursion and associated extinction events in the Prague Basin (Czech Republic). *Bulletin of Geosciences*, **93**(3), 369–400.

<https://doi.org/10.3140/bull.geosci.1710>

Meyer, K.M. and Kump, L.R. 2008. Oceanic euxinia in earth history: Causes and consequences. *Annual Reviews Earth and Planetary Science Letters*, **36**, 251-288.

<https://doi.org/10.1146/annurev.earth.36.031207.124256>

Morford, J.L. and Emerson, S. 1999. The geochemistry of redox sensitive trace metals in sediments. *Geochimica et Cosmochimica Acta*, **63**, 1735-1750.

[https://doi.org/10.1016/S0016-7037\(99\)00126-X](https://doi.org/10.1016/S0016-7037(99)00126-X)

Munnecke, A., Samtleben, C. and Bickert, T. 2003. The Ireviken Event in the lower Silurian of Gotland, Sweden — relation to similar Palaeozoic and Proterozoic events.

*Palaeogeography Palaeoclimatology Palaeoecology*, **195**, 99-124.

[https://doi.org/10.1016/S0031-0182\(03\)00304-3](https://doi.org/10.1016/S0031-0182(03)00304-3)

Owens, J.D., Gill, B.C., Jenkyns, H.C., Bates, S.M., Severmann, S., Kuypers, M.M.M., Woodfine, R.G. and Lyons, T.W. 2013. Sulfur isotopes track the global extent and dynamics of euxinia during Cretaceous Oceanic Anoxic Event 2. *Proceedings of the National Academy of Sciences*, **110**, 18407-18412. <https://doi.org/10.1073/pnas.1305304110>

Owens, J.D., Lyons, T.W., Hardisty, D.S., Lowery, C.M., Lu, Z., Lee, B. and Jenkyns, H.C. 2017. Patterns of local and global redox variability during the Cenomanian-Turonian Boundary Event (Ocean Anoxic Event 2) recorded in carbonates and shales from central Italy. *Sedimentology*, **64**, 168-185. <https://doi.org/10.1111/sed.12352>

Owens, J.D., Reinhard, C.T., Rohrssen, M., Love, G.D. and Lyons, T.W. 2016. Empirical links between trace metal cycling and marine microbial ecology during a large perturbation to Earth's carbon cycle. *Earth and Planetary Science Letters*, **449**, 407-417.

<https://doi.org/10.1016/j.epsl.2016.05.046>

Pasquier, V., Bryant, R.N., Fike, D.A. and Halevy, I. 2021. Strong local, not global, controls on marine pyrite sulfur isotopes. *Science Advances*, **7**, eabb7403.

<https://doi.org/10.1126/sciadv.abb7403>

Poulton, S.W. and Canfield, D.E. 2005. Development of a sequential extraction procedure for iron: implications for iron partitioning in continentally derived particulates. *Chemical Geology*, **214**, 209-221. <https://doi.org/10.1016/j.chemgeo.2004.09.003>

Present, T.M., Paris, G., Burke, A., Fischer, W.W. and Adkins, J.F. 2015. Large Carbonate Associated Sulfate isotopic variability between brachiopods, micrite, and other sedimentary components in Late Ordovician strata. *Earth and Planetary Science Letters*, **432**, 187-198. <https://doi.org/10.1016/j.epsl.2015.10.005>

Railsback, L.B., Holland, S.M., Hunter, D.M., Jordan, E.M., Diaz, J.R. and Crowe, D.E. 2003. Controls on Geochemical Expression of Subaerial Exposure in Ordovician Limestones from the Nashville Dome, Tennessee, U.S.A. *Journal of Sedimentary Research*, **73**, 790-805. <https://doi.org/10.1306/020503730790>

Raiswell, R. and Canfield, D.E. 1998. Sources of iron for pyrite formation in marine sediments. *American Journal of Science*, **298**, 219-245. <https://doi.org/10.2475/ajs.298.3.219>

Raiswell, R., Hardisty, D.S., Lyons, T.W., Canfield, D.E., Owens, J.D., Planavsky, N.J., Poulton, S.W. and Reinhard, C.T. 2018. The iron paleoredox proxies: A guide to the pitfalls, problems and proper practice. *American Journal of Science*, **318**, 491-526. <https://doi.org/10.2475/05.2018.03>

Raiswell, R., Newton, R., Bottrell, S.H., Coburn, P.M., Briggs, D.E.G., Bond, D.P.G. and Poulton, S.W. 2008. Turbidite depositional influences on the diagenesis of Beecher's Trilobite Bed and the Hunsrueck Slate: Sites of soft tissue pyritization. *American Journal of Science*, **308**, 105-129. <https://doi.org/10.2475/02.2008.01>

Richardson, J.A., Newville, M., Lanzirrotti, A., Webb, S.M., Rose, C.V., Catalano, J.G. and Fike, D.A. 2019. Depositional and diagenetic constraints on the abundance and spatial variability of carbonate-associated sulfate. *Chemical Geology*, **523**, 59-72. <https://doi.org/10.1016/j.chemgeo.2019.05.036>

Rölich, P. 2007. Structure of the Prague Basin: The deformation diversity and its causes (the Czech Republic). *Bulletin of Geosciences*, **82**, 175-182. <https://doi.org/10.3140/bull.geosci.2007.02.175>

Rose, C.V., Fischer, W.W., Finnegan, S. and Fike, D.A. 2019. Records of carbon and sulfur cycling during the Silurian Ireviken Event in Gotland, Sweden. *Geochimica et Cosmochimica Acta*, **246**, 299-316. <https://doi.org/10.1016/j.gca.2018.11.030>

Rudnick, R.L. and Gao, S. 2003. The Composition of the Continental Crust. In: Holland, H.D. and Turekian, K.K. (eds), *Treatise on Geochemistry, Vol. 3, The Crust*, Elsevier-Pergamon, 1-64. <http://dx.doi.org/10.1016/b0-08-043751-6/03016-4>

Saltzman, M.R. 2001. Silurian delta C-13 stratigraphy: A view from North America. *Geology*, **29**, 671-674. [https://doi.org/10.1130/0091-7613\(2001\)029<0671:SCSAVF>2.0.CO;2](https://doi.org/10.1130/0091-7613(2001)029<0671:SCSAVF>2.0.CO;2)

Saltzman, M.R. 2002. Carbon isotope ( $\delta^{13}\text{C}$ ) stratigraphy across the Silurian-Devonian transition in North America: evidence for a perturbation of the global carbon cycle. *Palaeogeography Palaeoclimatology Palaeoecology*, **187**, 83-100. [https://doi.org/10.1016/S0031-0182\(02\)00510-2](https://doi.org/10.1016/S0031-0182(02)00510-2)

Saltzman, M.R. and Thomas, E. 2012. Carbon Isotope Stratigraphy. In: Goldstein, F.M., Ogg, J.G. and Schmitz, M. (eds). *The Geologic Time Scale 2012*, 207-267. <https://doi.org/10.1016/B978-0-444-59425-9.00011-1>

Scotese, C.R. 2014. Atlas of Silurian and Middle-Late Ordovician Paleogeographic Maps (Mollweide Projection), Maps 73-80. *The Early Paleozoic, PALEOMAP Atlas for ArcGIS Vol. 5*. Evanston, IL. <https://doi.org/10.13140/2.1.1087.2324>

Sepkoski Jr., J.J. 1996. Patterns of Phanerozoic extinction: a perspective from global databases. In: Walliser, O.H. (ed). *Global Events and Event Stratigraphy in the Phanerozoic*, 35-51. Springer-Verlag, Berlin. [https://doi.org/10.1007/978-3-642-79634-0\\_4](https://doi.org/10.1007/978-3-642-79634-0_4)

Sim, M.S. 2019. Effect of sulfate limitation on sulfur isotope fractionation in batch cultures of sulfate reducing bacteria. *Geosciences Journal*, **23**, 687-694. <https://doi.org/10.1007/s12303-019-0015-x>

Sim, M.S., Ono, S. and Hurtgen, M.T. 2015. Sulfur isotope evidence for low and fluctuating sulfate levels in the Late Devonian ocean and the potential link with the mass extinction event. *Earth and Planetary Science Letters*, **419**, 52-62. <https://doi.org/10.1016/j.epsl.2015.03.009>

Slavík, L., Štorch, P., Manda, Š. and Frýda, J. 2014. Integrated stratigraphy of the Ludfordian in the Prague Synform. *Geologiska Föreningens i Stockholm Förhandlingar*, **136**, 238-242. <https://doi.org/10.1080/11035897.2013.851733>

Sproson, A.D, Pogge von Strandmann, P. A. E., Selby, D., Jarochovska, E., Frýda, J., Hladil, J., Loydell, D. K., Slavík, L., Calner, M., Maier, G., Munnecke, A. and Lenton, T.M. 2022. Osmium and lithium isotope evidence for weathering feedbacks linked to orbitally paced organic carbon burial and Silurian glaciations. *Earth and Planetary Science Letters*, **577**, 117260. <https://doi.org/10.1016/j.epsl.2021.117260>

Stampfli, G.M., Raumer, J.F. and Borel, G.D. 2002. Paleozoic evolution of pre-Variscan terranes: From Gondwana to the Variscan collision. *Geological Society of America Special Paper* **364**, 263-280. <https://doi.org/10.1130/0-8137-2364-7.263>

Štorch, P. 1995. Upper Silurian (upper Ludlow) graptolites of the *N. inexpectatus* and *N. kozłowskii* biozones from Kosov Quarry near Beroun (Barrandian area, Bohemia). *Bulletin of Geosciences Czech Geological Survey*, **70**, 65-89.

Štorch, P. 1998. VIII. Volcanism. In: Chlupáč, I., Havlíček, V., Kříž, J., Kukul, Z. and Štorch, P. (eds). *Paleozoic of the Barrandian (Cambrian to Devonian)*. Czech Geological Survey, 149-164.

Stricanne, L., Munnecke, A. and Pross, J. 2006. Assessing mechanisms of environmental change: Palynological signals across the Late Ludlow (Silurian) positive isotope excursion ( $\delta^{13}\text{C}$ ,  $\delta^{18}\text{O}$ ) on Gotland, Sweden. *Palaeogeography Palaeoclimatology Palaeoecology*, **230**, 1-31. <https://doi.org/10.1016/j.palaeo.2005.07.003>

Suchy, V., Sykorová, I., Stejskal, M., Šafanda, J., Machovič, V. and Novotná, M. 2002. Dispersed organic matter from Silurian shales of the Barrandian Basin, Czech Republic: optical properties, chemical composition, and thermal maturity. *International Journal of Coal Geology*, **53**, 1-25. [https://doi.org/10.1016/S0166-5162\(02\)00137-4](https://doi.org/10.1016/S0166-5162(02)00137-4)

Swart, P.K. and Eberli, G. 2005. The nature of the  $\delta^{13}\text{C}$  of periplatform sediments: Implications for stratigraphy and the global carbon cycle. *Sedimentary Geology*, **175**, 115-129. <https://doi.org/10.1016/j.sedgeo.2004.12.029>

- Talent, J.A., Mawson, R., Andrew, A.S., Hamilton, P.J. and Whitford, D.J. 1993. Middle Paleozoic extinction events: Faunal and isotopic data. *Palaeogeography Palaeoclimatology Palaeoecology*, **104**, 139-152. [https://doi.org/10.1016/0031-0182\(93\)90126-4](https://doi.org/10.1016/0031-0182(93)90126-4)
- Tasáryová, Z., Schnabl, P., Čížková, K., Pruner, P., Janoušek, V., Rapprich, V., Štorch, P., Manda, Š. Frýda, J. and Trubac, J. 2014. Gorstian palaeoposition and geotectonic setting of Suchomasty Volcanic Centre (Silurian, Prague Basin, Teplá-Barrandian Unit, Bohemian Massif). *Geologiska Föreningens i Stockholm Förhandlingar*, **136**, 262-265. <https://doi.org/10.1080/11035897.2013.879735>
- Tasáryová, Z., Janoušek, V. and Frýda, J. 2018. Failed Silurian continental rifting at the NW margin of Gondwana: evidence from basaltic volcanism of the Prague Basin (Teplá-Barrandian Unit, Bohemian Massif). *International Journal of Earth Science*, **107**, 1231-1266. <https://doi.org/10.1007/s00531-017-1530-5>
- Taylor, S.R. and McLennan, S.M. 1995. The geochemical the continental evolution crust. *Reviews in Mineralogy and Geochemistry*, **33**, 241-265.
- Tonarová, P., Eriksson, M.E. and Hints, O. 2012. A jawed polychaete fauna from the late Ludlow Kozłowski event interval in the Prague Basin (Czech Republic). *Bulletin of Geosciences Czech Geological Survey*, **87**, 713–732. <https://doi.org/10.3140/bull.geosci.1317>
- Tribovillard, N., Algeo, T.J, Lyons, T.W. and Ribolleau, A. 2006. Trace metals as paleoredox and paleoproductivity proxies: An update. *Chemical Geology*, **232**, 12-32. <https://doi.org/10.1016/j.chemgeo.2006.02.012>
- Urbanek, A. 1993. Biotic crises in the history of the upper Silurian graptoloids: a paleobiological model. *Historical Biology*, **7**, 29-50. <https://doi.org/10.1080/10292389309380442>
- Vacek, F. and Žák, J. 2019. A lifetime of the Variscan orogenic plateau from uplift to collapse as recorded by the Prague Basin, Bohemian Massif. *Geological Magazine*, **156**, 485-509. <https://doi.org/10.1017/S0016756817000875>
- Wotte, T., Shields-Zhou, G.A. and Strauss, H. 2012. Carbonate-associated sulfate: Experimental comparisons of common extraction methods and recommendations toward a standard analytical protocol. *Chemical Geology*, **326-327**, 132-144. <https://doi.org/10.1016/j.chemgeo.2012.07.020>

Young, S.A., Benayoun, E., Kozik, N.P., Hints, O., Martma, T., Bergström, S.M. and Owens, J.D. 2020. Marine redox variability from Baltica during extinction events in the latest Ordovician-early Silurian. *Palaeogeography Palaeoclimatology Palaeoecology*, **553**, 109792. <https://doi.org/10.1016/j.palaeo.2020.109792>

Young, S.A., Kleinberg, A. and Owens, J.D. 2019. Geochemical evidence for expansion of marine euxinia during an early Silurian (Llandovery-Wenlock boundary) mass extinction. *Earth and Planetary Science Letters*, **513**, 187-196. <https://doi.org/10.1016/j.epsl.2019.02.023>

Zhang, F., Frýda, J., Fakhraee, M., Lin, Y., Wei, G.-Y., Cao, M., Li, N., Zhou, J., Frýdová, B., Wei, H. and Shen, S. 2022. Marine anoxia as a trigger for the largest Phanerozoic positive carbon isotope excursion: evidence from carbonate barium isotope records. *Earth and Planetary Science Letters*, **584**, 117421. <https://doi.org/10.1016/j.epsl.2022.117421>

## Figure Captions

Fig. 1: (A) Paleogeographic reconstruction of the late Silurian (~425 Ma; modified from Scotese, 2014). (B) Distribution of the rocks of the Barrandian Terrane in the central Bohemian Region of the present-day Czech Republic with the Mušlovka and Kosov Quarry sections highlighted with yellow circles (modified from Frýda et al. 2021a).

Fig. 2: Schematic diagram of the marine redox proxies used in the present study. Proxies are in order of their relative sensitivity to redox conditions based on the marine redox ladder. Appropriate lithology for each proxy is denoted by grey background pattern (bricks – carbonate; dashes – shale/mudstone). Threshold values for iodine-to-calcium ratios (I/Ca) from Lu et al. (2016); manganese (Mn) concentrations from Morford and Emerson (1999); vanadium (V) concentrations from Rudnick and Gao (2003); uranium (U) and molybdenum (Mo) concentrations from McLennan (2001); iron speciation ( $Fe_T/Al$ ,  $Fe_{HR}/Fe_T$ ,  $Fe_{pyr}/Fe_{HR}$ ) from Raiswell et al. (2008), Raiswell and Canfield (1998), and März et al. (2008). Threshold value for Mn represents the average oxic marine sediments and values for V, U, and Mo are upper continental crust values. \*Threshold values correspond to upper continental crust values, concentrations above which likely indicate reducing condition. ♦Threshold value corresponds to modern oxic sediment values, concentrations notably below which are indicative of reducing conditions.

Fig. 3: (A) Field photo of massively to thinly bedded mud-, wacke-, and packstones in the lower portion of the Kopanina Formation exposed in Mušlovka Quarry section. (B & C) Hand samples from the flat-pebble conglomerate intervals in the Mušlovka Quarry section. Flat-pebble clasts are purple-pink within light-brown matrix; possible microbial laminations surrounding some flat pebbles are traced with dashed lines. (D) Thin section photomicrograph from the Mušlovka Quarry section showing the boundary between a wackestone flat-pebble conglomerate clast and dolomitized matrix, arrows point toward clast (8.5 m). (E) Thin section photomicrograph from the Mušlovka Quarry section; example of finely disseminated pyrite in dolomitized matrix (7.5 m – plane light). (F) Field photo of upper and lower sections of the interbedded shales and limestones of the Kopanina Formation at Kosov Quarry. (G) Field photo of the upper section at Kosov Quarry showing thinly bedded shale interspersed in more massively bedded carbonates.

Fig. 4: Stratigraphic column and geochemical data for the Mušlovka Quarry section, Prague, Czech Republic. (A) Carbonate and organic carbon isotope data (carbonate carbon isotope data from Lehnert et al., 2003, 2007). (B) Carbonate-associated sulfate and pyrite sulfur isotope data. (C) Total organic carbon and pyrite concentration data. (D) I/(Ca+Mg) ratio data from both micritic matrix and flat-pebble conglomerate clasts. The Lau/Kozłowski extinction is highlighted in light yellow. Biozonation from Chadimova et al. (2015). Carb: carbonate; org: organic; CAS: carbonate-associated sulfate; pyr: pyrite; *Neocuc. inexpect.*: *Neocucullograptus inexpectatus*; *Pr. dubius postfrequens*: *Prisiograptus dubius postfrequens*; *P. latilobus*: *Pseudomonoclimacis latilobus*; *S. balticus*: *Slovenograptus*.

Fig. 5: Stratigraphic column and geochemical data for the Kosov Quarry section, Beroun, Czech Republic. (A) Organic carbon isotope data (additional carbonate and organic carbon isotope data from Frýda et al. 2021a). (B) Pyrite sulfur isotope data (additional data from Frýda et al. 2021a). (C) TOC concentration data. The Lau/Kozłowski extinction is highlighted in light yellow. Carb: carbonate; org: organic; pyr: pyrite; *N. inexpectatus*: *Neocucullograptus inexpectatus*; *N. kozłowski*: *Neocucullograptus kozłowski*; *P. latilobus*: *Pseudomonoclimacis latilobus*; *S. balticus*: *Slovenograptus balticus*; *P. fragmentalis*: *Pristiograptus fragmentalis*; *Po. siluricus*: *Polygnathoides siluricus*; *O. snajdri*: *Ozarkodina snajdri*; *P. latialata*: *Pedavis latialata*; *O. crispa*: *Ozarkodina crispa*.

Fig. 6: Stratigraphic column and geochemical data for the Kosov Quarry section, Beroun, Czech Republic. (A) Highly reactive (HR) to total (T) iron (Fe) ratios. (B) Pyrite (pyr) to

highly reactive iron ratios. (C) Total iron to aluminum (Al) ratios. (D) Manganese (Mn) concentrations. (E) Vanadium (V) concentrations. (F) Uranium (U) concentrations. (G) Molybdenum (Mo) concentrations. The Lau/Kozlowski extinction is highlighted in light yellow; CC: carbonate corrected, TOC: total organic carbon, UCC: upper continental crust; see Fig. 5 caption for graptolite & conodont biozones.

Fig. 7: Cross plots for the assessment of possible diagenetic alteration of carbon, oxygen, and sulfur isotopes and I/Ca values in the Mušlovka Quarry shallow shelf carbonate section. (A)  $\delta^{18}\text{O}_{\text{carb}}$  vs.  $\delta^{13}\text{C}_{\text{carb}}$ . (B)  $\delta^{13}\text{C}_{\text{carb}}$  vs. I/Ca. (C)  $\delta^{18}\text{O}_{\text{carb}}$  vs. I/Ca. (D)  $\delta^{18}\text{O}_{\text{carb}}$  vs. [CAS]. (E)  $\delta^{13}\text{C}_{\text{carb}}$  vs.  $\delta^{34}\text{S}_{\text{CAS}}$ . (F)  $\delta^{18}\text{O}_{\text{carb}}$  vs.  $\delta^{34}\text{S}_{\text{CAS}}$ . Modeling results from Lau and Hardisty (2022) are also presented in most panels, showing changes in carbon, oxygen, and sulfur isotopes and I/Ca values based on varying diagenetic conditions. The yellow diamond represents starting composition in the model. The lines represent sediment- (solid) and fluid-buffered (dashed) conditions for diagenesis with meteoric water (brown), reducing seawater (red), and oxic seawater (blue). Arrows represent traditional interpretations for redox proxies in the absence of diagenetic overprinting.

Fig. 8: Cross plot of uranium and molybdenum enrichment factors for Kosov Quarry based on plots from Algeo and Tribovillard (2009). Blue symbols show data from this study, green symbols show corresponding data from Frýda et al. (2021b). Diagonal dashed lines represent seawater (SW) Mo/U ratio of  $\sim 7.5 - 7.9$  and fractions thereof.

Fig. 9: Schematic drawing of extent of anoxia through time along an idealized transect of the semi-restricted Prague Basin based on proxy data. Approximate locations of Mušlovka and Kosov Quarry sections are marked by stars. Reducing conditions in both the water column and sediment porewaters are represented by transparent purple overlay. See text for discussion and compare with the model in Frýda et al (2021b, fig. 9). CIE: carbon isotope excursion.

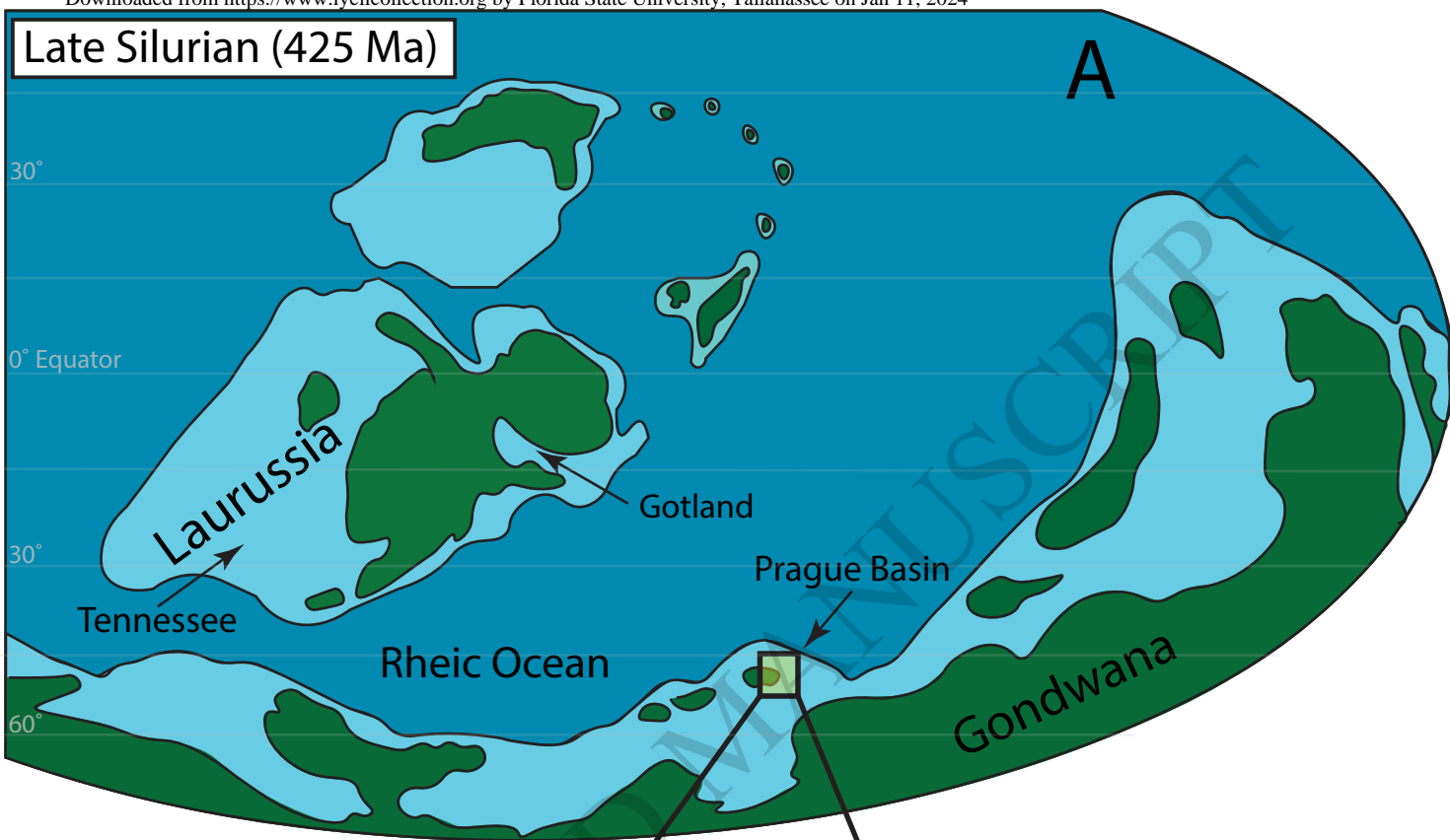
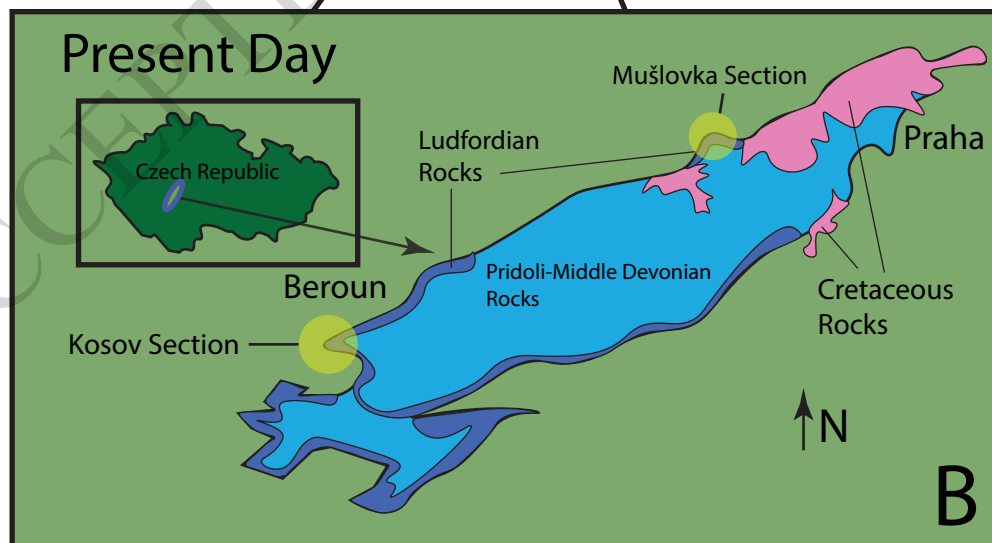


Figure 1



Manganese Reduction  
Nitrate Reduction  
Oxygen Reduction  
Iron Reduction  
Sulfate Reduction

Proxy

Relative Thresholds

I/Ca	oxic > 2.6 suboxic 0-2.6 $\mu\text{mol/mol}$
[Mn]	anoxic-suboxic* < 850 ppm
[V]	anoxic-suboxic* > 97 ppm
[U]	anoxic* > 2.8 ppm
Fe <sub>T</sub> /Al	anoxic > 0.64
Fe <sub>HR</sub> /Fe <sub>T</sub>	anoxic > 0.38
Fe <sub>pyr</sub> /Fe <sub>HR</sub>	ferruginous < 0.6 euxinic > 0.8
$\delta^{34}\text{S}_{\text{SO}_4}$	higher magnitude excursion = more pyrite burial
[Mo]	anoxic-euxinic* > 1.5 ppm

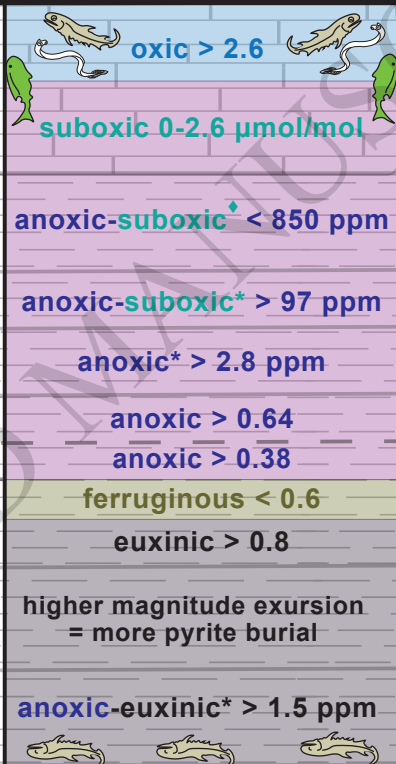
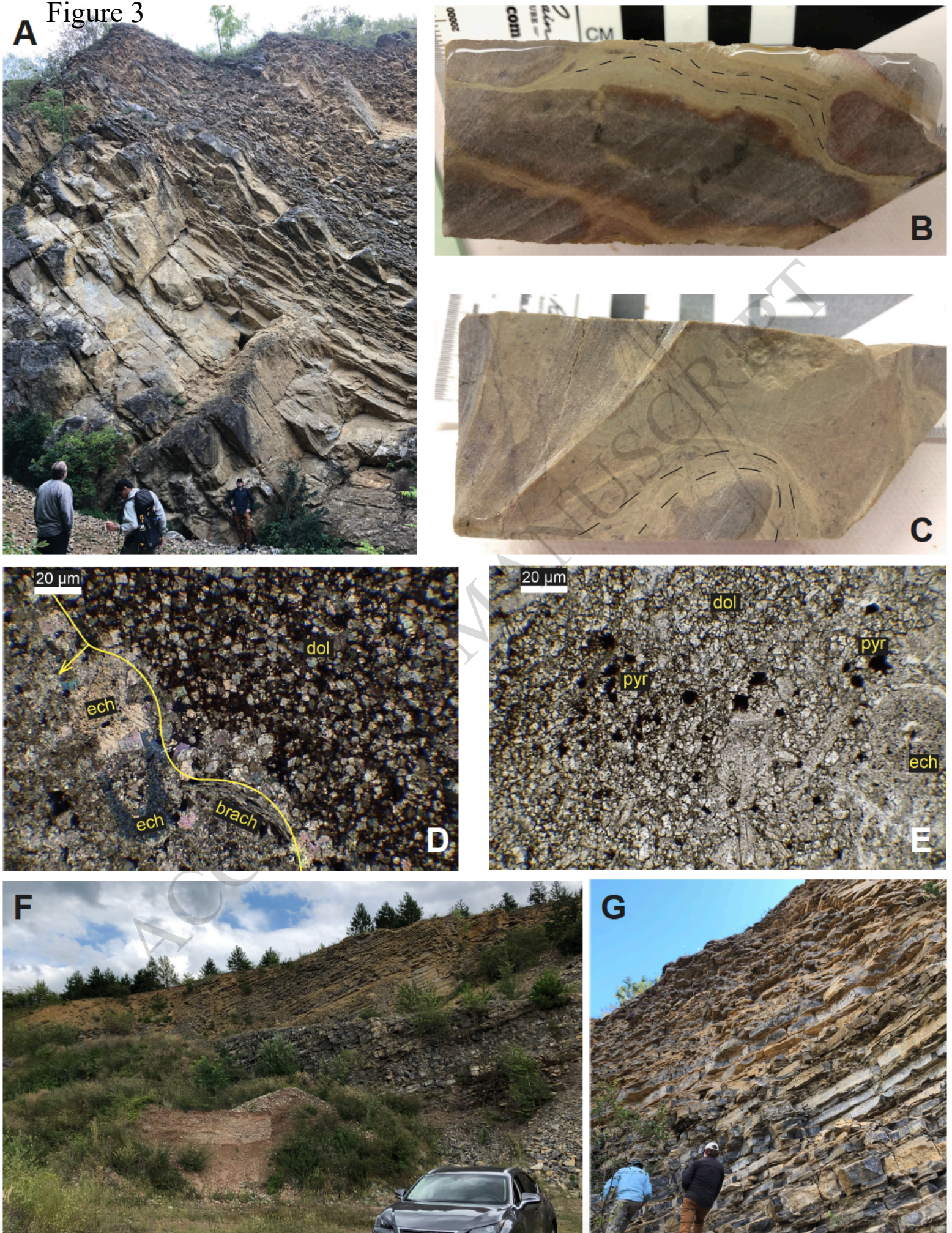


Figure 3



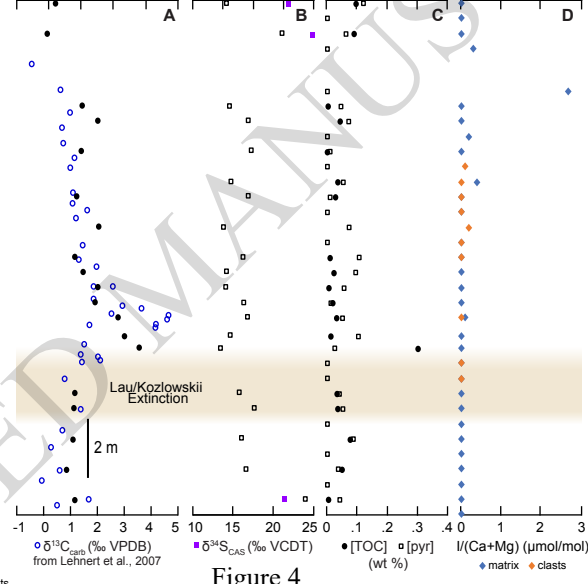
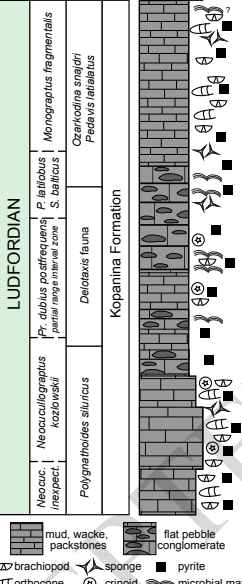


Figure 4

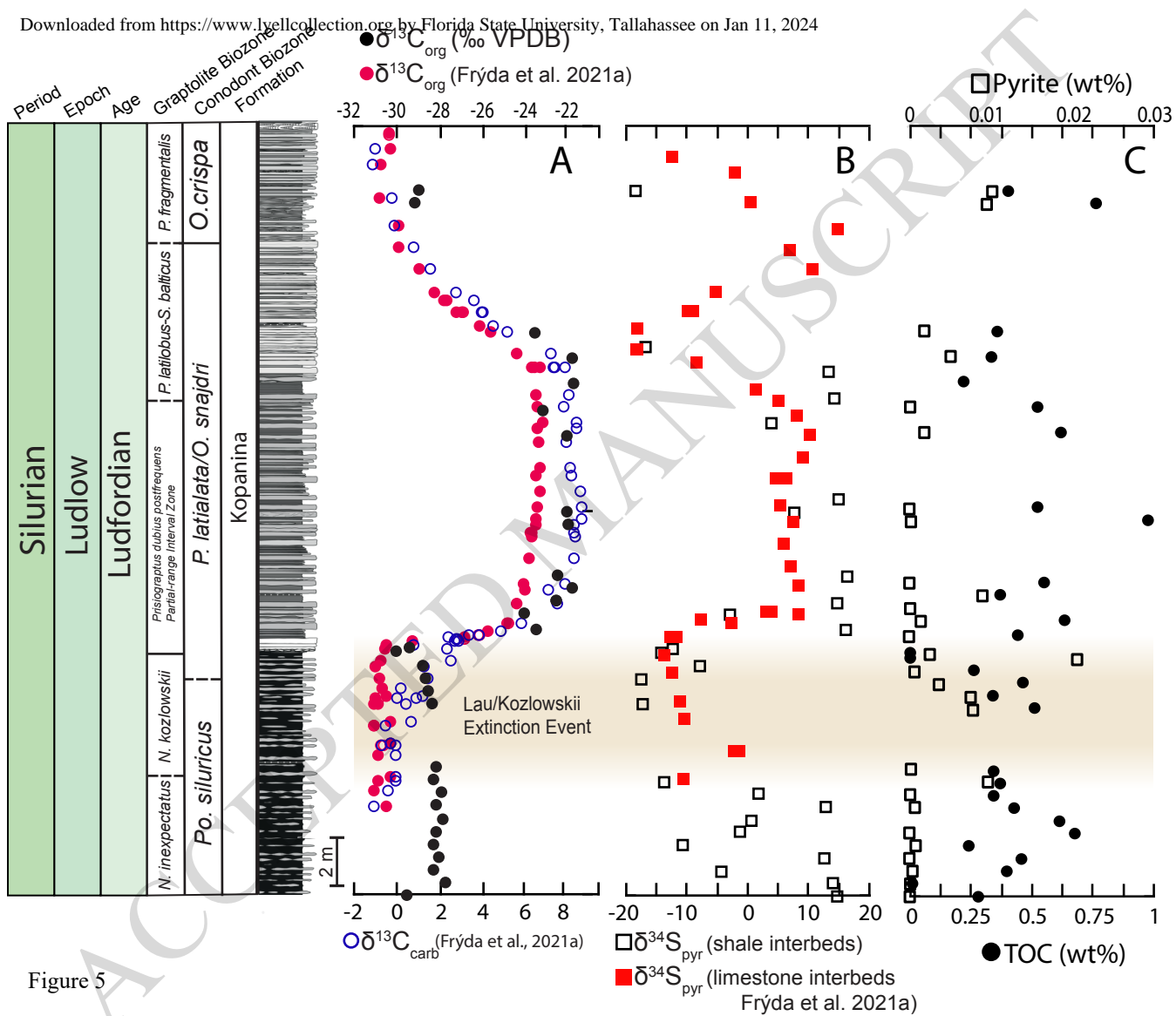


Figure 5

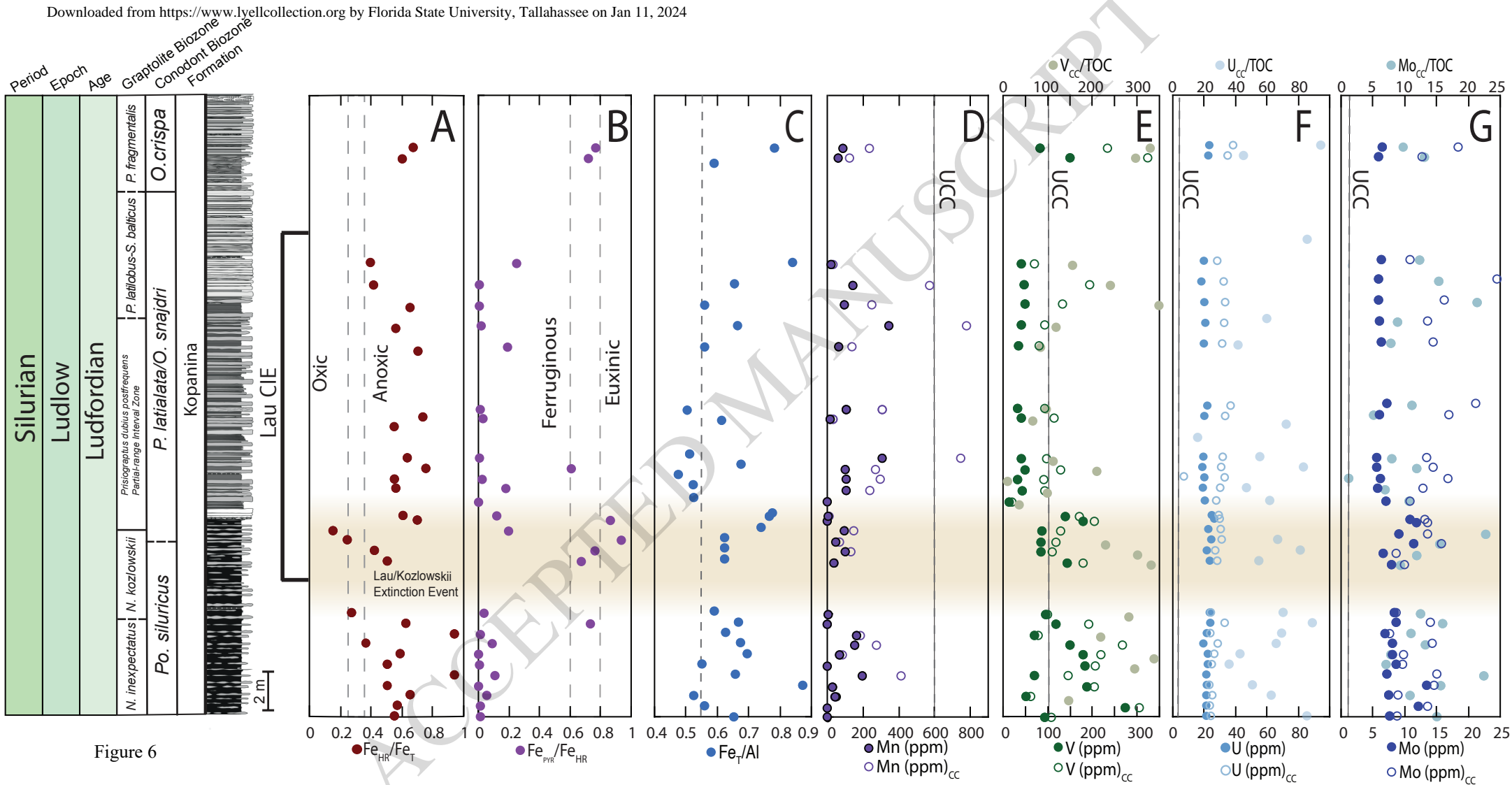


Figure 6

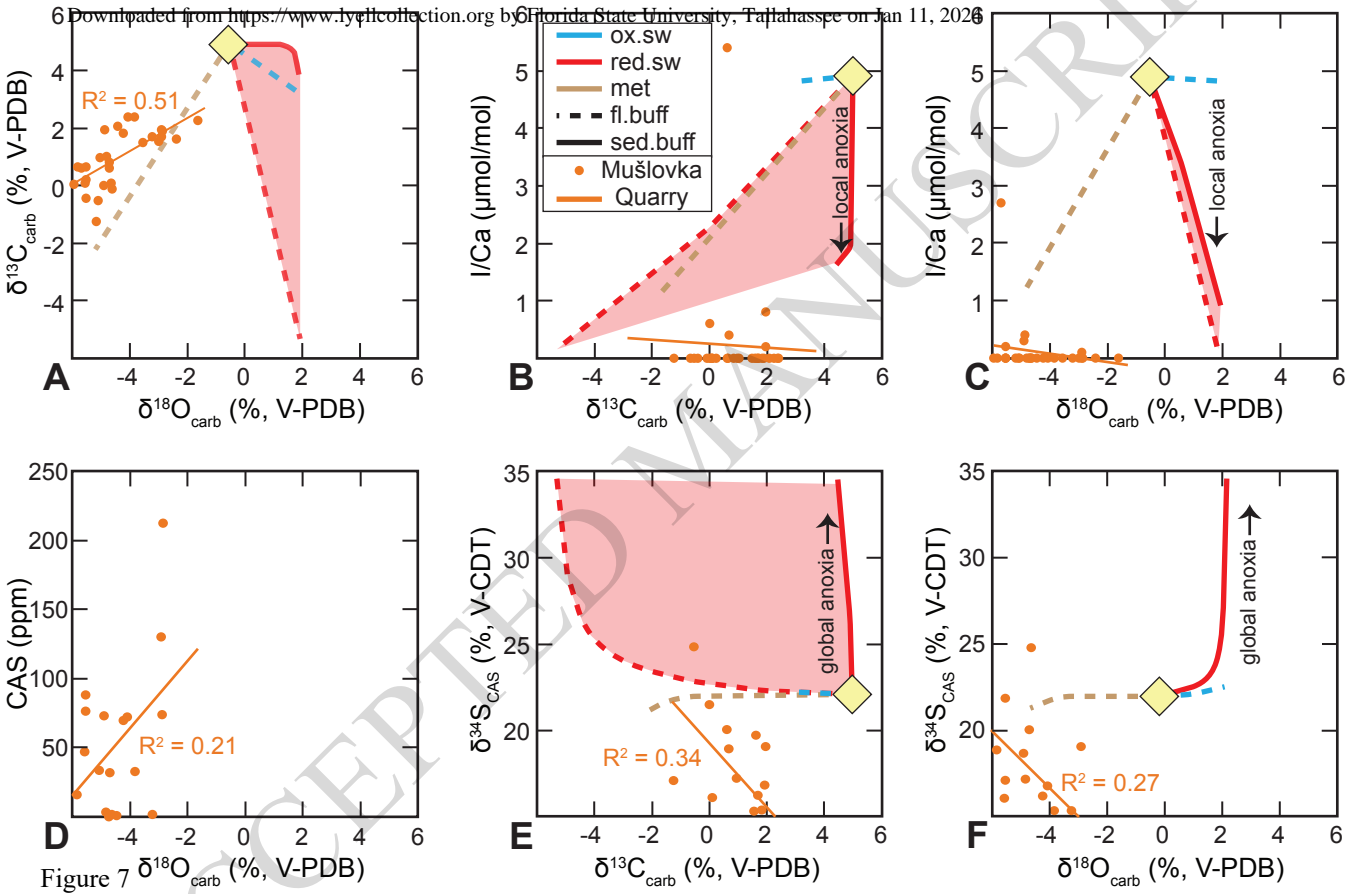
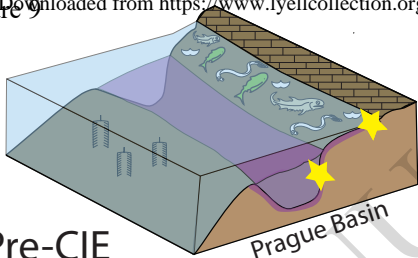


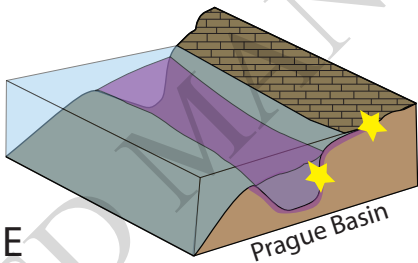
Figure 7



A.



B.



C.

